

FINAL REPORT FOR AN ULTRA-LOW NOISE HIGH GAIN PHOTODETECTOR FOR ATOM COUNTING



Troy Barrie
Greg Davis

Project Sponsors:
Dr. Kirk Madison, Dr. James Booth, Dr. Bruce Klappauf

Applied Science 479
Engineering Physics
University of British Columbia
January 12th, 2009

Project 0868

Abstract

Magneto-optical traps (MOT) fluoresce at varying optical powers that are linearly dependent on the number of atoms in the MOT. Detecting this fluorescence precisely and consistently is important for studying the behaviour of MOTs, and for accurately measuring relative atom counts in a MOT affected by a specific experimental event.

This project developed a photodetector specifically designed for such measurements for Dr. Kirk Madison, Dr. James Booth, and Dr. Bruce Klappauf. The application requires a photodetector with low noise, high gain, wide dynamic range, and good bandwidth. Target specifications for the final product were: signal to noise ratio greater than 40 dB, bandwidth greater than 10 kHz, selectable gain allowing accurate optical power measurement from 10 nW to 10 μ W, and use of a 1 cm² photodiode.

The characterization results showed measurement capability covering the full specified range, and minimum signal to noise ratio of 43 dB with typical signal to noise ratios significantly higher (50 dB and greater). Four selectable gain stages of 100 M Ω , 50 M Ω , 10 M Ω , and 1 M Ω were included to allow precision measurement at all powers of interest. The 100 M Ω gain stage is intended for DC high precision measurement with a bandwidth less than 10 Hz but excellent noise performance (1 mV RMS noise), the 50 M Ω gain stage is intended for high sensitivity fast measurements and has a bandwidth of 2.5 kHz and noise of 8 mV RMS, the 10 M Ω gain stage has a bandwidth of 17 kHz and noise of 5 mV RMS, and the 1 M Ω gain stage has a bandwidth of 60 kHz and noise of 1.8 mV RMS. The detector achieves the signal to noise ratio required at all powers, and nearly achieves the bandwidth targets for the full power range, but at the lowest power of interest, does not achieve the bandwidth and noise specification simultaneously. Each detector employs a 1 cm² FDS1010 photodiode for detection and includes an iris, mounting cage, and shielding case.

Full calibration at 780 nm has been completed for the first detector, and less detailed calibration has been completed for the other detectors.

Table of Contents

Abstract	ii
1 Background	1
2 Discussion	3
2.1 Objectives	3
Electrical Specifications.....	3
Mechanical Specifications	3
2.2 Theory	4
2.2.1 Transimpedance Amplifier	4
2.3 Design Process	8
2.3.1 Simple Transimpedance Amplifier	9
2.3.2 Two Stage Amplifier.....	10
2.3.3 Differential Amplifier	12
2.3.4 Bootstrapped Cascode.....	13
2.3.5 Passive Component Selection	14
2.3.6 Housing Design.....	15
2.4 Measurement Procedure.....	17
2.4.1 Photodiode Responsivity vs. Position of Incident Light.....	18
2.4.2 Noise	19
2.4.3 Frequency Response	19
2.4.4 Photodetector Power Calibration	20
2.4.5 Problems and Limitations	21
2.5 Results.....	22
2.5.1 Photodiode Responsivity vs. Position.....	23
2.5.2 First Iteration Simple Prototype.....	23
2.5.3 First Iteration Two Stage Prototype	26
2.5.4 Differential Prototype	28
2.5.5 Second Design Iteration.....	30
2.5.6 Final Design Selection	31
2.5.7 Final Circuit, 1 pF Feedback Capacitance	32
2.5.8 Final Photodetector	34
3 Conclusions.....	42
4 Recommendations.....	44
Appendix A: Prototype Schematics	45
Appendix B: Final Schematic and PCB Layout	51
Appendix C: Laser Driver Board.....	53
Appendix D: Power Calibration Curves	54
References.....	68

List of Tables

Table 1 Simple prototype first iteration RMS noise, $C_F = 4.7$ pF.....	25
Table 2 Two stage prototype dark current output with -5 V bias on photodiode	28
Table 3 Two stage prototype first iteration RMS noise, $C_F = 10$ pF.....	28
Table 4 Differential prototype RMS noise, $C_F = 4.7$ pF	30
Table 5 Simple prototype second iteration results, $C_F = 0$	30
Table 6 Final circuit comparison of RMS noise levels, $C_F = 1$ pF.	33
Table 7 Final circuit noise comparison with different feedback capacitors, OPA381.....	34
Table 8 Final detector gain resistances, feedback capacitances, and switch positions	35
Table 9 Final detector bandwidth and noise summary.....	36

List of Figures

Figure 1 Basic operation of a MOT ^[9]	1
Figure 2 Model of a photodiode.....	4
Figure 3 Transimpedance amplifier	5
Figure 4 Transimpedance amplifier noise model.....	6
Figure 5 Noise and signal gain in the transimpedance amplifier	7
Figure 6 Two op amp single gain stage design.....	10
Figure 7 Gain curves of the two stage circuit	11
Figure 8 Differential design	13
Figure 9 Bootstrapped Cascode	14
Figure 10 Mechanical design drawing of detectors in the system.	16
Figure 11 Optical system used for characterization and calibration measurements.	18
Figure 12 Simple prototype schematic and first iteration frequency response	24
Figure 13 Two stage prototype schematic and first iteration frequency response.....	27
Figure 14 Differential prototype schematic and frequency response	29
Figure 15 Final design basic schematic	32
Figure 16 Final circuit frequency response, OPA380, $C_F = 1$ pF.	33
Figure 17 Final detector frequency response	35
Figure 18 Power calibration curve for Detector 2, 780 nm, 1 M Ω gain.	37
Figure 19 Power calibration curve for Detector 2, 780 nm, 10 M Ω gain.	38
Figure 20 Power calibration curve for Detector 2, 780 nm, 50 M Ω gain.	39
Figure 21 Power calibration curve for Detector 2, 780 nm, 100 M Ω gain.	40
Figure 22 Simple prototype first iteration schematic.....	45
Figure 23 Two stage prototype first iteration schematic.....	46
Figure 24 Differential prototype schematic.	47
Figure 25 Simple prototype second iteration schematic.	48
Figure 26 Two stage prototype second iteration schematic.	49
Figure 27 Bootstrapped cascode prototype schematic.....	50
Figure 28 Final circuit schematic.....	51
Figure 29 Final PCB layout	52
Figure 30 Laser driver schematic.....	53

Figure 31 Detector 1 Power Calibration Curves.....	55
Figure 32 Detector 3 Power Calibration Curves.....	57
Figure 33 Detector 4 Power Calibration Curves.....	59
Figure 34 Detector 5 Power Calibration Curves.....	61
Figure 35 Detector 6 Power Calibration Curves.....	63
Figure 36 Detector 7 Power Calibration Curves.....	65
Figure 37 Detector 8 Power Calibration Curves.....	67

1 Background

Electronic applications frequently require amplification of an input signal originating from a sensor or actuator. Depending upon the application, the amplifier can be optimized to maximize either bandwidth or signal to noise ratio (SNR). In many cases, bandwidth and SNR come as a trade-off; an increase in bandwidth results in a decrease in SNR, and vice versa. Thus, each amplifier must be tuned to fit the desired electrical specifications for the particular end application.

For this project, fluorescent light from atoms in a magneto-optical trap (MOT) is collected onto a photodiode. The optical power of the fluorescence typically ranges from nanowatts to microwatts, leading to the requirement of a transimpedance amplifier to amplify the photocurrent and convert it to an output voltage. A MOT is a laser cooling device in which momentum imparted to atoms by photons from lasers is used to restrict the movement of atoms. This effect, utilized in conjunction with a magnetic field, forces all of the atoms in the MOT to become trapped in a small volume. The result is an atom cloud cooled to a few hundred micro-Kelvins and confined by radiation pressure. When the atoms decay from an excited state to a ground state, they emit photons, generating fluorescence whose intensity can be measured to monitor the behaviour and quantity of the atoms in the MOT. A simplified conceptual outline of a MOT is shown in Figure 1.

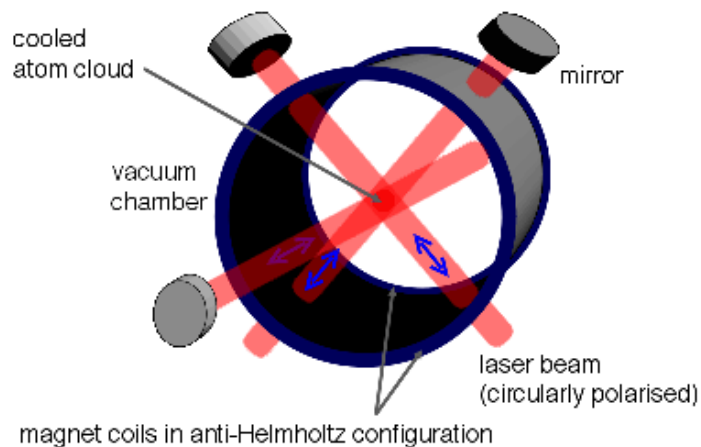


Figure 1 Basic operation of a MOT ^[9]

In order for the MOT to operate, the lasers used for atomic cooling must be tuned close to an atomic absorption frequency (wavelength) specific to the type of atom being cooled and trapped. For this project, lithium atoms and rubidium atoms are being trapped, dictating the wavelengths – 671 nm and 780 nm, respectively – at which the photodiode must be calibrated.

The desired transimpedance amplifier should linearly amplify currents ranging from approximately 5 nA to 5 μ A and convert them to voltages that a mathematical model will interpret to determine the number of atoms within the atom-cloud. A prototype of such a transimpedance amplifier was designed and built by a previous student^[6]. This model uses a simplistic design, intended as an early exploration into the concept, but lacks the high performance and permanence that motivate the objectives of this project. The crux of the problem is the trade-off between maximizing the SNR while maintaining a high bandwidth, and ensuring the full range of potential input photocurrents can be accurately measured. The gain for the existing model is achieved using a 10 M Ω resistor; this converts a 10 nA input signal to a 10 mV output signal. Capacitors within the circuit must balance the capacitance of the photodiode to minimize noise gain and ensure stability, yet still allow for high frequency signals to be amplified. The complications of the signal bandwidth/noise gain trade-off are explained further in Section 2.1.1.

The project was sponsored by Dr. Kirk Madison and Dr. Bruce Klappauf of UBC Physics, and BCIT visiting scientist Dr. James Booth. Commercial solutions are available, but due to the high cost of these products, the fact that multiple detectors are required, and the specific requirements and narrow application demands of the project, a significantly cheaper in-house design was a viable and more attractive solution. For example, two suitable commercial products are the Newport 1931-C high performance low power optical meter, which costs \$2400, and the Thorlabs PDA50B amplified photodetector, which costs \$469 and lacks the large area photodiode desired for the project. The initial breadboard prototype completed earlier is currently in use in the lab, but the project sponsors require a higher performance, fully characterized, calibrated, permanent solution.

2 Discussion

2.1 Objectives

The primary objective of the project was to build eight photodetectors for measuring fluorescence from Rubidium and Lithium magneto-optical traps. The detectors also were to be calibrated and integrated into the optical systems in which they will be used. To achieve the necessary level of precision, sensitivity, and performance, electrical specifications were defined for the photodetector circuits; to allow integration into optical systems and provide integration versatility, mechanical specifications were defined for the housing of the photodetectors.

Electrical Specifications

- Optical power detection range 10 nW-10 μ W
- Minimum 40 dB Signal to Noise Ratio throughout detection range
- Large area photodiode (1 cm²)
- Able to connect to 5-pin standardized lab power input (+/-5V, +/-15V, GND)
- Output to standard BNC cable
- Minimum 10 kHz bandwidth
- Selectable gain

Mechanical Specifications

- Physically fit into the system (as small as possible)
- Include Thorlabs optical mount with rails and 1 inch diameter threaded hole
- Include iris
- Include one inch diameter optical bandpass filter

The calibration and characterization of the detectors was also an important objective. Characterization includes establishing the frequency response and noise level of the detector for each selectable gain stage. Calibration consists of defining the relationship between the input optical power at the photodiode and the output voltage level.

2.2 Theory

To detect optical power using a photodiode, one must measure the current emitted by the photodiode accurately. The simplest way to do this is to connect the photodiode to a resistor, converting the photocurrent directly to an easily measurable voltage. This achieves an extremely low noise specification (the only noise sources are the Johnson noise of the load resistor and the shot noise of the photodiode), but there are two problems with this circuit. First, the voltage across the load resistor appears across the photodiode. Since most photodiodes' responsivity is dependent on the voltage across the diode, this results in non-linear output. The second, more critical problem results from the capacitance of the photodiode itself. A photodiode can be modelled as a parallel combination of a current source, a capacitor, and a resistor, as shown in Figure 2.

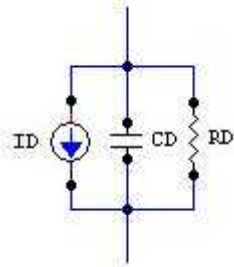


Figure 2 Model of a photodiode. The capacitance of the diode causes problems when trying to take fast measurements.

Because the full voltage swing of the signal appears also across the capacitor C_D , the interaction between the capacitance of the photodiode and the load resistor limit the bandwidth of the signal. One way of solving this problem is to use a transimpedance amplifier.

2.2.1 Transimpedance Amplifier

The simplest version of the transimpedance amplifier is shown in Figure 3.

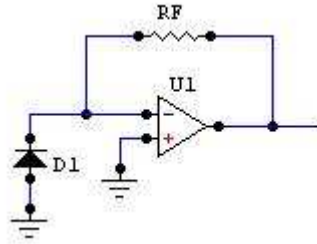


Figure 3 Transimpedance amplifier. Forcing the cathode of the photodiode to virtual ground by connecting it to an op amp allows the frequency response of the transimpedance amplifier to be expanded by limiting the voltage swing across the diode capacitance.

The most important feature of the transimpedance amplifier is that it maintains the cathode of the photodiode D_1 at virtual ground because it is connected to the non-inverting input of the operational amplifier U_1 . This means that the voltage swing of the output signal across the feedback resistor R_F no longer appears across the capacitance of the photodiode C_D in the model of Figure 2. As the photocurrent changes, U_1 changes its output to shift the voltage at the cathode of the photodiode back to ground. Thus, the bandwidth limit imposed by the interaction between the load resistor R_F and the capacitance of the photodiode C_D has been mitigated. The cost of this bandwidth improvement is the added noise that results from the addition of an active component. A model of the transimpedance amplifier and its noise sources is shown in Figure 4. I_D , the photocurrent, I_{NS} , the shot noise of the photocurrent, and I_J , the Johnson noise of R_F , are all treated the same way by the circuit, and thus can be modelled in parallel as shown. The diode shunt resistance in the model of Figure 3 has been omitted because in practice, for a Silicon photodiode this resistance is so large that it has no effect on the operation of the circuit.

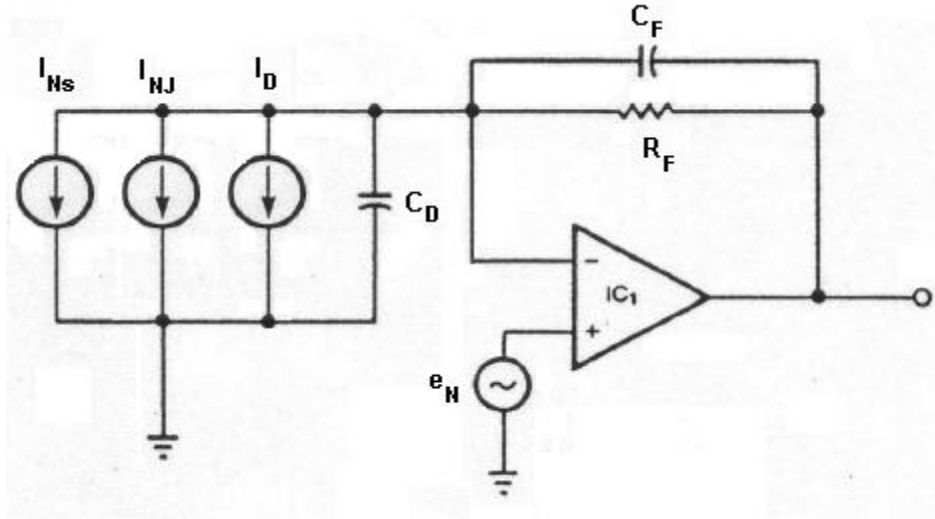


Figure 4 Transimpedance amplifier noise model. The shot noise N_S , Johnson noise N_J of the gain resistor R_F , and signal current I_D are all treated the same by the amplifier. The voltage noise of the amplifier e_N is amplified according to the closed loop gain of the op amp.

The amplifier voltage noise e_N is amplified by the non-inverting closed loop gain of the op amp. The loop gain A_{Vcl} is given by ^[12]

$$A_{Vcl} = \frac{A_{Vol}}{1 + \frac{A_{Vol}}{1+j\omega C_D Z_F}}$$

where Z_F is the complex impedance of the combination of R_F and C_F , and A_{Vol} is the open loop gain of the op amp. This noise gain has a pole at the RC frequency defined by the interaction between C_D and R_F , resulting in the noise gain peaking phenomenon. This noise gain levels off at the same place that the signal begins to roll off; that is, the zero in the transfer function caused by the RC interaction of R_F and C_F . The noise gain does not roll off until the bandwidth limit of the op amp is reached, before which it is amplified by an amount proportional to C_D/C_F . Essentially, this noise gain peaking means that high frequency amplifier noise dominates the total noise, and the larger the photodiode capacitance, the larger the effect of the noise gain peaking. The noise gain and signal gain of the transimpedance amplifier are shown in Figure 5.

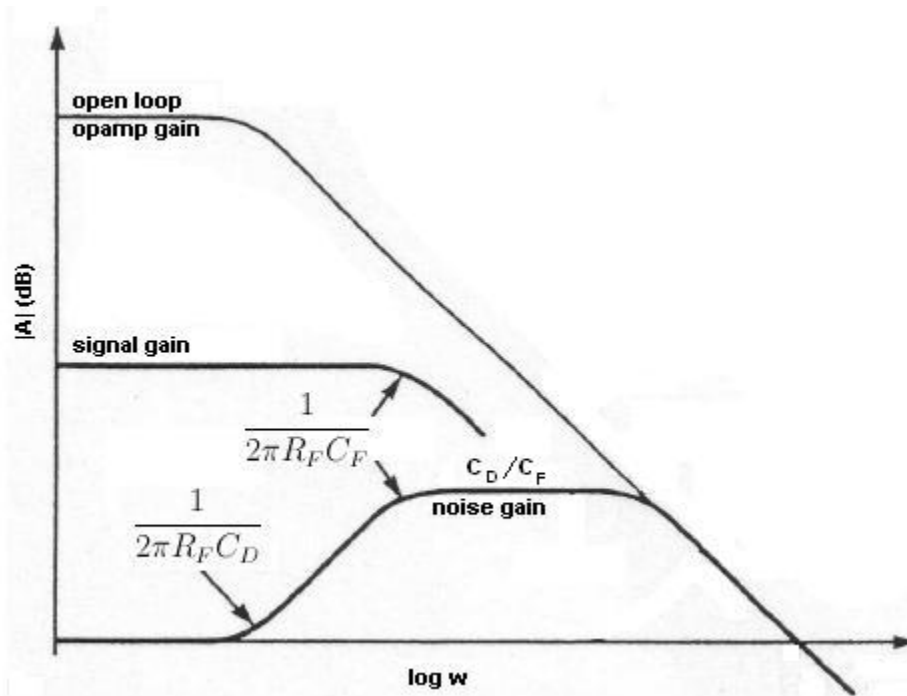


Figure 5 Noise and signal gain in the transimpedance amplifier. The signal gain rolls off beginning at the RC corner frequency defined by the feedback resistance and capacitance. The noise gain defined by the closed loop op amp gain has a pole at the RC corner frequency defined by the feedback resistor interacting with the photodiode capacitance, causing the noise gain to rise until it hits a zero at the RC corner where the signal gain begins rolling off. Above this frequency, the noise gain is constant at a ratio defined by the ratio of the feedback capacitance and the diode capacitance until it is rolled off by the op amp open loop gain limit.

This noise amplification effect can result in poor signal to noise ratio, or in some cases oscillation of the op amp. Careful op amp selection and PCB layout are critical for getting the best performance possible for the application.

Examining Figure 5, it is clear that increasing the feedback capacitance will reduce the effect of noise gain peaking by shifting the zero of the noise gain curve left by reducing the corner frequency $1/2\pi R_F C_F$, thus reducing the peak level of the noise gain. However, this comes at the expense of also reducing the bandwidth of the amplifier. In the limit that the feedback capacitance matches the diode capacitance, the noise gain effect is completely eliminated and the shot noise and Johnson noise physical limit is reached, as in the case of the simple load resistor current to voltage converter; however, the

bandwidth is also reduced to the same low level as the simple load resistor, so nothing has been gained. The challenge, then, is to find an optimal circuit that will trade off bandwidth and noise to achieve a level that meets the specifications of the specific application.

A circuit based on the transimpedance amplifier described above consists of the final design of the photodetector for this project.

2.3 Design Process

The primary challenge of designing an amplifier to meet the specifications set out in the project objectives stemmed from the combination of reconciling the very high sensitivity required with the extremely large area photodiode, which carries with it an obese capacitance of over 300 pF^[4] at a bias voltage of -5 V. Maintaining a good signal to noise ratio and salvaging as much bandwidth as possible with such high amplification and diode capacitance was the major obstacle.

In order to overcome the challenge, several possible circuits were designed, fabricated, and tested. In the first stage of prototyping, three designs were prototyped: the simple transimpedance amplifier described in Section 2.2.1, a two stage amplifier employing two op amps in combination in a single gain stage, and a differential design intended to optimize common mode rejection. After this, a second prototyping stage was undertaken, which included second iteration designs of the simple and two stage designs with slight modifications, and a new design based around a bootstrapped cascode. The prototype boards were fabricated using the LPKF milling machine in the UBC Engineering Physics Project Lab.

After all the circuits had been tested, the simple transimpedance amplifier was selected as the final design based on the testing results. The circuit design was then tweaked, and a final printed circuit board (PCB) layout was created to be professionally fabricated. The

housing for the circuit and PCB layout were designed together to meet the mechanical specifications outlined in the project objectives.

2.3.1 Simple Transimpedance Amplifier

The first design was the basic transimpedance amplifier shown in Figure 3. The full schematic of the first iteration of this design is included in Appendix A. The design included power regulation and decoupling, as well as four selectable gain resistors ranging from 10 k Ω to 10 M Ω .

Selection of the op amp in this design is crucial. The op amp should have very low input noise, low input currents, and low offset voltage. The Texas Instruments OPA381 is specifically designed for transimpedance amplifiers, and made a suitable selection ^[4]. A second, very similar op amp with the identical pinout to the OPA381, the OPA380 ^[19], was also tested in this circuit. The primary difference between the two op amps is the gain bandwidth product (GBW): the OPA380 has a GBW of 90 MHz, while the OPA381 has a GBW of 18 MHz. In the case of this project, because the bandwidth of the signal is limited not by the op amp gain bandwidth product, but by the roll off caused by the RC interaction of the feedback resistor and capacitor, the wider bandwidth OPA380 is not necessary. In fact, the OPA381 performs better, because its narrower bandwidth limits the spectrum available for noise gain peaking, rolling off the noise gain curve earlier (see Figure 5).

This circuit was also designed to include a variable bias voltage on the photodiode that could be tuned with a potentiometer to range from 0 to -15 V. The bias voltage design included a minor error, however, which was corrected in the second iteration of the design. The design required a voltage buffer between the voltage divider used to set the bias voltage and the photodiode itself, which was missing in the first iteration design. Biasing the photodiode has two major effects: first, by applying a voltage across the photodiode, the capacitance of the diode is reduced, reducing the effect of the noise gain peaking; second, a voltage across the photodiode results in a photocurrent being emitted

even when there is no incident light; this current is called dark current. The second iteration of the simple prototype also improved power supply regulation and decoupling, and added individual feedback capacitors for each feedback resistor.

2.3.2 Two Stage Amplifier

In an effort to improve noise performance without sacrificing bandwidth, a second circuit incorporating two op amps was designed. A simplified schematic is shown in Figure 6. The full schematic is shown in Appendix A.

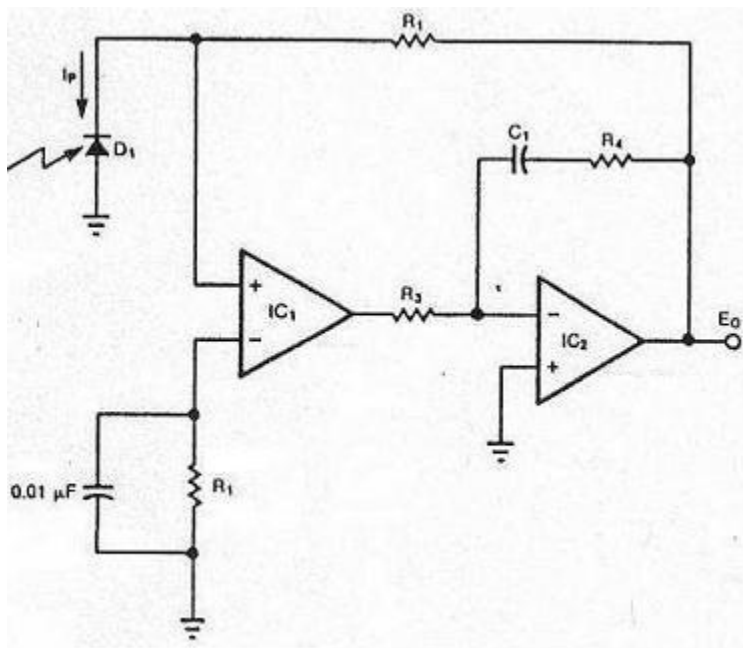


Figure 6 Two op amp single gain stage design ^[1]. The integrator like response of the internal feedback loop formed by C_1 and R_4 creates a modified open loop gain curve that limits the bandwidth available for noise gain without limiting the signal bandwidth.

In this case, the first op amp IC_1 should be very low noise, while the second op amp IC_2 can be used to effectively limit the open loop bandwidth of the overall amplification scheme to something just above the signal bandwidth. This eliminates the problem of noise gain peaking at frequencies above the maximum signal frequency without limiting signal bandwidth, provided that the modified open loop gain remains above the RC frequency of the feedback resistor and capacitor. To demonstrate this effect, one can qualitatively describe what happens at different frequencies. At low frequency, C_1 is

effectively an open circuit, and the open loop gain is the product of the gain of IC₁ and the gain of IC₂. However, at high frequencies, C1 becomes a short, and the open loop gain is limited by the gain affected by the internal feedback network of R₃ and R₄. By keeping R₃ larger than R₄, high frequencies will be attenuated. With correct component selection, this design can allow the full signal bandwidth to remain unaffected, while shifting the amplifier bandwidth limit back to roll off the noise gain peaking earlier and limit the spectrum of the noise gain. This effect is seen graphically in Figure 7.

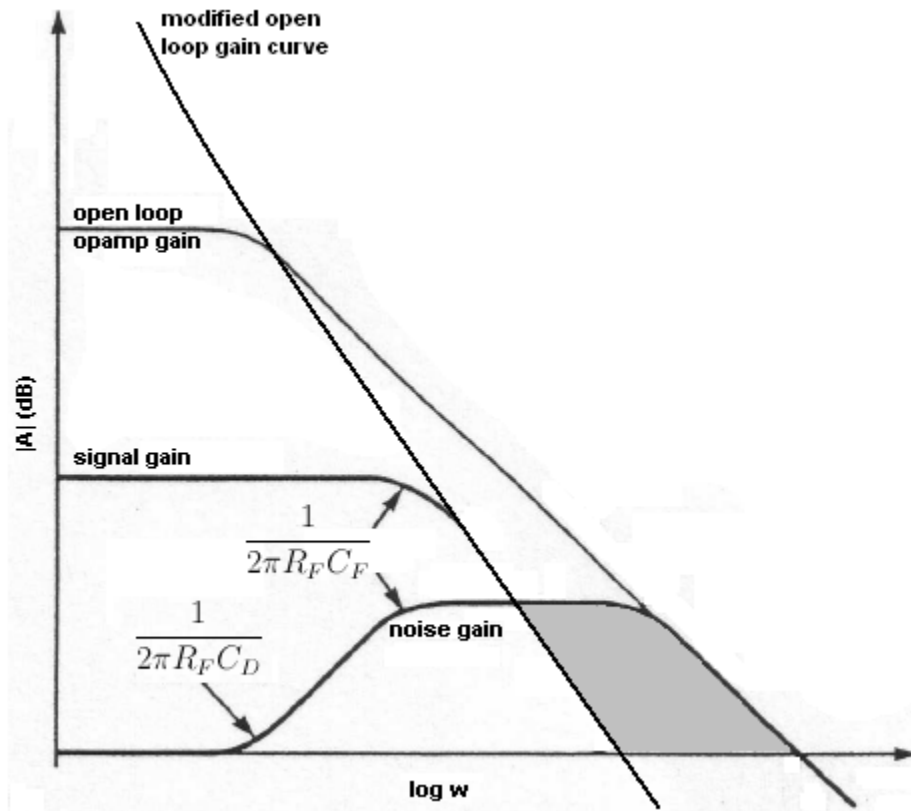


Figure 7 The modified open loop gain curve of the two stage circuit eliminates the bandwidth that amplifies only noise (shaded gray) without affecting signal bandwidth.

For the first op amp, IC₁, the OPA381 again made a suitable choice. For the second op amp, IC₂, a wider bandwidth op amp with less restrictive noise specifications was selected: the OPA656 [5].

This circuit also included variable bias voltage, and selectable gain resistors, as in the simple design. The same bias voltage error was present in this circuit as in the simple circuit, and it was also corrected in the second prototype iteration. Power supply regulation and decoupling was also improved in the second iteration, individual feedback capacitors for each feedback resistor were added, and two different op amps were selected for trial. IC₁ was replaced by the AD8655^[15], and IC₂ was replaced by the AD8027^[16].

2.3.3 Differential Amplifier

The third design is shown in Figure 8 (full schematic in Appendix A). In this design, two matched op amps provide equal amplification of the photocurrent, and the output of each is fed into an instrumentation amplifier. This configuration utilizes the high common mode rejection ratio of the instrumentation amplifier to eliminate noise common to both signals. This is especially useful in rejecting power supply noise, electrostatic noise, and magnetically coupled noise. This design requires careful trace length matching and layout of components to be equidistant from sources of potential noise.

For this design, IC₁ and IC₂ were on a dual op amp chip, the AD8626^[17], and the instrumentation amplifier was the AD8221^[18].

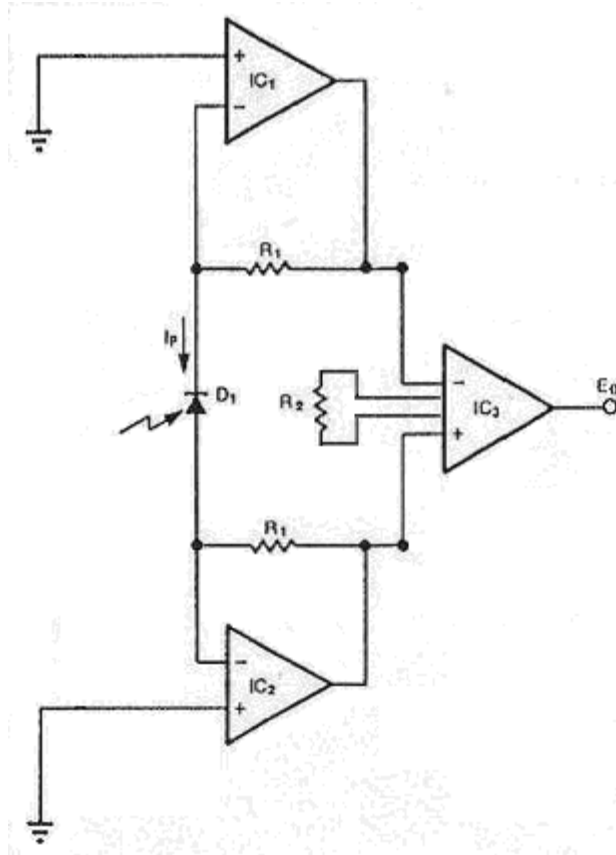


Figure 8 Differential design. The instrumentation amplifier IC₃ has a high common mode rejection ratio, eliminating noise common to the circuit such as electrostatically and magnetically coupled noise and power supply noise.

2.3.4 Bootstrapped Cascode

After the first iteration of prototypes, a fourth design was added. The bootstrapped cascode^[12] uses a bipolar junction transistor to isolate the diode capacitance from the feedback network of the op amp. This eliminates the noise gain peaking problem while adding only a small amount of noise due to the transistor. The design is shown in Figure 9, and the full schematic is in Appendix A.

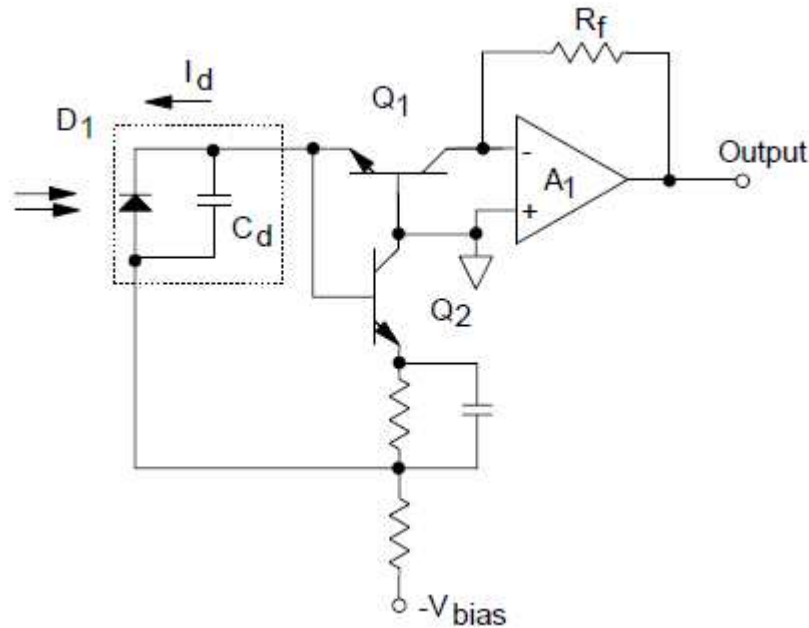


Figure 9 Bootstrapped Cascode ^[10]. The transistor Q1 isolates the photodiode capacitance C_D from the amplifier, eliminating noise gain and allowing higher bandwidth.

In this design, Q1 transmits the photocurrent to the feedback resistor, but acts as a buffer to separate the photodiode capacitance from the feedback network. In order to linearize Q1, a small bias current at the base is needed. This is provided by Q2. Unfortunately, the bias current required to linearize Q1 is larger than the photocurrent itself for the low range of power detection, saturating the amplifier at high gain stages.

2.3.5 Passive Component Selection

The most critical part of component selection in this project is finding an appropriate op amp, but choosing suitable passives is also important.

Most importantly, choosing the best feedback resistors is key to producing a detector that will not drift or degrade over time. High precision is good, but stability is much more important. Metal film and thick film through-hole resistors provide the best performance characteristics. Metal film and thick film resistors are the least likely to have manufacturing or damage defects, which can lead to 1/f pink noise in addition to Johnson

noise ^[14]. They also generally provide the best stability and thermal drift characteristics ^[12].

Also, choosing suitable capacitors is important. In this case, shunt resistance, stability, and performance at different frequencies is the key. For the feedback capacitors, stability, precision, and excellent performance throughout the frequency spectrum is important. To achieve this, COG/NP0 ceramic capacitors were used ^[12]. COG/NP0 capacitors are manufactured from specific dielectric materials to have minimal temperature dependence, vibration induced noise injection, and loss, and excellent high frequency performance.

For decoupling, precision and stability are less critical, but covering the frequency spectrum is important. Low frequency high amplitude spikes must be eliminated equally as well as high frequency white noise. To achieve this, a combination of capacitors was employed. To handle the low frequency and high voltage noise, large polarized electrolytic capacitors were used on the power supply inputs. Electrolytic capacitors have low shunt resistance and perform poorly at higher frequencies, however. To help in this area, 10 μ F tantalum capacitors and 0.1 μ F ceramic capacitors were also used on the power supply inputs, voltage regulator inputs and outputs, and op amp power supply pins. Tantalum capacitors handle all frequencies relatively well, and ceramic capacitors are particularly good at higher frequencies ^[12].

2.3.6 Housing Design

The completed photodetector system is intended to be mounted, at close range, onto the MOT unit in the sponsor's lab. The light emanating from the MOT is focused through a 10 cm length 2.5 cm diameter tube by a lens, after which the light is divided by a beam splitter and the two paths each enter photodetectors.

Figure 10 below shows a SolidWorks drawing of the photodetector mount system. The physical specifications required the complete system (lens tube, beam splitter and two

photodetectors) to fit the MOT unit and have a clear line of sight to the atom cloud. Minimum sizing was not set, but was desired to be as small as possible. The housing unit purchased was bought as a stock manufactured aluminum shielding case and modified to add the necessary holes using the project lab's water jet cutter. The beam splitter cube is the largest component and set the critical size maximum for the housing. The circuit board was designed to its minimum size and set parallel to the face of the beam splitter cube to further reduce additional volume.

The photodetector was attached using cage mounts, which serve two purposes: it provides a rigid mounting surface that ensures structural stability, and allows for up to 1.5 cm of travel in order for the light source to be focused sharply on the photodiode. The cage mounts were attached to the aluminum housing by sunken threaded machined holes in the Thorlabs cage mount component. Drawings of the housing system are included below in Figure 10.

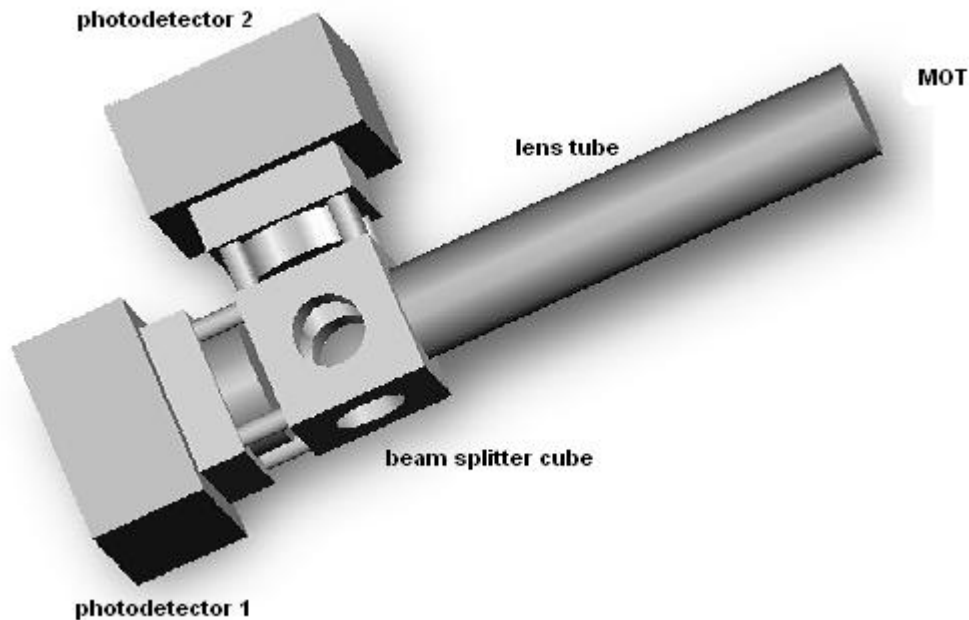


Figure 10 Mechanical design drawing of detectors in the system.

2.4 Measurement Procedure

Careful and consistent measurements are crucial to establishing reliable performance metrics and achieving accurate calibration. As such, the techniques used to obtain the results presented in Section 2.5 are outlined here. The optical system used to produce the signal used in the measurement of the noise, frequency response, and power calibration is shown in Figure 11. The beam splitters (approximately 5% reflectivity) and neutral density filter (approximately 12% transmission) were used to reduce the power of the beam to suitable levels for the detector while remaining in a clean, linear region of the laser output. The beam splitter was also used to produce a second beam incident on a second, commercial photodetector made by New Focus ^[13]. This detector, labelled “NF photodetector” in Figure 11, is a 125 MHz flat frequency response Silicon photodiode photodetector used as a reference in the frequency response measurement. The current driver used was a custom device with a tunable output current and an AC modulation input. The modulation input, however, has a bandwidth limit of approximately 50 kHz. To achieve laser modulation above this frequency, a simple custom laser driver board was made to accept both a DC current and an AC voltage to modulate the laser voltage directly. The schematic and explanation of this laser driver is contained in Appendix C. The noise and frequency response measurements were performed with a 780 nm optical bandpass filter installed on the detector.

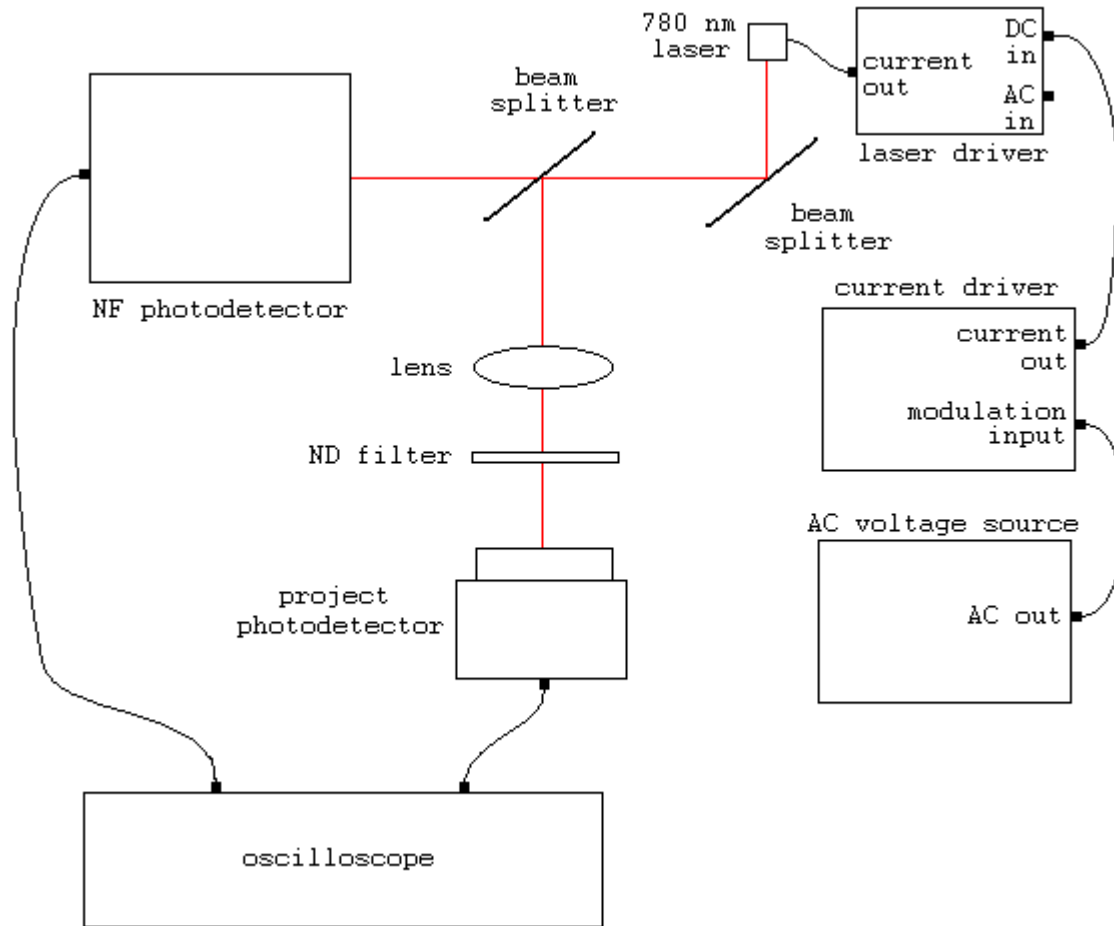


Figure 11 Optical system used for characterization and calibration measurements.

2.4.1 Photodiode Responsivity vs. Position of Incident Light

Some photodiodes exhibit non-uniform responses across their detection area. To quantify this non-uniformity for the FDS1010 photodiode used in this project, a 780 nm semiconductor laser was focused onto a specific part of the photodiode, and the voltage across the photodiode was measured directly using an oscilloscope as the position of the photodiode was systematically varied. To avoid obfuscating the results by using an amplifier, the photodiode was connected directly to the oscilloscope inputs to measure the photodiode response. The photodetector was mounted on an x-y-z stage used to move the photodiode slowly across the focused beam location, and the output was measured at each positional increment across the cross sectional detection area of the photodiode.

The behaviour of the photodiode corresponding to variation in incident beam spreading was also measured. The beam was focused at the centre of the photodiode, and the stage was used to move the photodiode away from the focal plane, spreading the light intensity across a successively larger area of the photodiode. The output was measured at several positions to determine if, as expected, it remained constant while the full beam remained on the photodiode detection area.

2.4.2 Noise

For each prototype and the final photodetector, the noise in each gain stage was measured. The noise level was measured using the digital oscilloscope to isolate the AC portion of the signal, which comprises the noise. The noise was measured at varying DC signals within the dynamic range of each gain stage. To provide the photodetector with a DC signal, the laser was driven at a constant current, and the beam passed through the optical system shown in Figure 11. To vary the intensity seen at the detector, the neutral density filter was added or removed as necessary, and the iris at the detector partially closed to allow only part of the incident beam. This mitigates issues of optical noise on the laser varying at different input currents that were observed when the intensity at the detector was varied by changing the input current to the laser.

The noise levels quoted are root mean squared (RMS) voltages. The RMS voltage of the AC signal was measured using the built in function on the digital oscilloscope.

2.4.3 Frequency Response

The frequency response was measured by modulating the input to the 780 nm laser with varying modulation frequencies, from DC to 300 kHz, and comparing the detector output to that of a high bandwidth flat frequency response New Focus photodetector. Below 50 kHz, the modulation was achieved by connecting an AC voltage supply to the modulation input of the custom current driver used. Due to bandwidth limitations on the modulation

input of the current driver, above 50 kHz modulation was achieved instead by connecting the function generator to the custom built laser driver board AC input, which modulates the laser voltage directly. Further explanation of the laser driver board is included in Appendix C.

To measure the frequency response, the frequency of modulation was varied, and the AC amplitude of the output of both detectors recorded. The amplitude of modulation was measured using the built in amplitude measurement function of the digital oscilloscope. Then, at each modulation frequency, the amplitude of the project detector was divided by the amplitude of the reference detector. Normalizing the results to the lowest frequency measured and converting the results to decibels yields the results shown in Section 2.5.

In some cases, the full frequency response was not required, but only an estimate of the 3 dB bandwidth. In this case, a measurement of the relative AC amplitudes of the two detectors was taken at a very low frequency – typically 10 Hz – and the frequency was adjusted upwards until the relative amplitudes reach half of the initial value. This frequency is the 3 dB bandwidth.

2.4.4 Photodetector Power Calibration

Power calibration was a sensitive process, requiring careful attention to calibration of optical components and consistency in measurement techniques. To attenuate the optical signal to ranges useful for power calibration in all gain stages, several optical components were employed. In addition to the optical setup shown in Figure 11, two mirrors and a second lens were added so that the detector was facing away from the laser. This was done to minimize the amount of light resulting from reflection and diffraction of the laser outside the primary beam path incident on the detector. Also, several neutral density filters were placed in the beam path as needed to attenuate the optical signal to the desired range. The measurements were performed by reading the detector output, then placing the power metre directly in front of the detector and reading the power metre output. The power calibration was performed without the bandpass filter on the

photodetector, and without the neutral density filter attached to the power metre. Power calibration was performed at 780 nm.

2.4.5 Problems and Limitations

The most persistent problem during measurements was separating electrical noise from optical noise. Optical noise, in the context of characterizing a photodetector, is considered signal; however, isolating electrical noise from optical noise proved to be difficult. In particular, because of the very high sensitivity of the higher gain stages, optical noise in these stages can be inadvertently amplified, artificially inflating the noise level of the photodetector.

Sources of optical noise include lighting in the room, noise on the current source driving the laser, laser noise caused by competing modes with similar gain stochastically switching, and laser far field reaching the detector. Other external noise sources include inherent oscilloscope noise, electro-magnetic noise coupled into the cabling, and power supply noise. Power supply noise at 60 Hz and harmonics was visible on the output of the detector, but appeared to be a result of both noise on the detector itself, and noise on the laser driver transferring onto the laser output, and thus appearing as part of the signal.

Noise levels on the laser output were also observed to vary at different current set points, likely due to competing modes of nearly the same gain stochastically switching between each other resulting in fluctuating output power. To mitigate this problem, the laser was driven at a constant current observed to have consistently good noise performance, and the intensity at the detector varied by changing the diameter of the aperture to the photodiode with the iris so as to limit the amount of the beam incident on the photodiode.

Some difficulties were also encountered with the frequency response measurements. The modulation signal was obscured partially by noise on both the project photodetector and the reference photodetector, and the error on the measurements of the relative amplitudes of the modulation signal was high. The built in amplitude measurement function on the

digital oscilloscope was helpful, but exhibited some digital quantization noise, and in cases of low modulation amplitude, sometimes had trouble determining accurate amplitudes due to the noise on the signal. Establishment of the general trend and shape of the frequency responses and the 3 dB bandwidths was, however, a repeatable process.

The primary obstacle in power calibration was reaching all ranges of power necessary, and isolating background noise. Because of unusual laser behaviour in many ranges of input currents, achieving arbitrary input power by means of varying the input current alone was not possible. To achieve the required power range, optical attenuation using neutral density filters and beam splitters was used in conjunction with variable input current to vary the input power. A second problem was the background noise apparently caused by the far field of the laser; this problem was particularly prevalent at higher gain stages. When the detector was facing the laser, blocking the primary beam and varying the current at the laser resulted in clear, significant variation on the detector output corresponding directly to the changes in the laser current. To help eliminate this problem, mirrors were used to direct the beam back in the opposite direction from which it came so that the detector was facing away from the laser. This minimized the background noise caused by reflections and diffractions of the far field. Another problem encountered was the effect of the bandpass filter. The 780 nm optical bandpass filter attenuated the signal significantly (approximately 70%), reducing the sensitivity of the detector. Also, the orientation of the filter was measured to be very important to how much the signal was attenuated. The angle that the beam hit the filter severely affects the amount of light the filter allows to pass. To avoid this problem, the calibration was performed without the bandpass filter. To eliminate the effect of background noise away from 780 nm, and allow measurements at very low scale on the detector, the calibrations were performed in complete darkness.

2.5 Results

The different prototypes were evaluated and compared based primarily on three performance metrics: frequency response, noise, and reliability. The frequency response

and noise were measured quantitatively, while the reliability was evaluated by the authors qualitatively through careful observation and notation of glitches, such as oscillation, railed output, inconsistent output, or altogether failure to function.

The specified noise values are root mean squared (RMS) voltages, and unavoidably include some amount of optical noise which cannot be completely identified and isolated. Also, power supply noise at 60 Hz and its harmonics were present in some amount on all measurements, further artificially inflating the noise figures. This power supply noise is present both on the circuit itself, and as a modulation signal on the laser due to noise on the current supply driving the laser. This was determined by observing the output at high gain stages, where 60 Hz noise was present in significantly larger amounts than at lower gain stages, indicating that it is a part of the optical input signal being amplified.

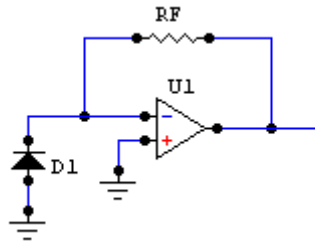
For these reasons, the noise performance of all circuits is in fact slightly better than specified; the values quoted are based on the total AC voltage superimposed on the DC signal, regardless of the source of the AC signal.

2.5.1 Photodiode Responsivity vs. Position

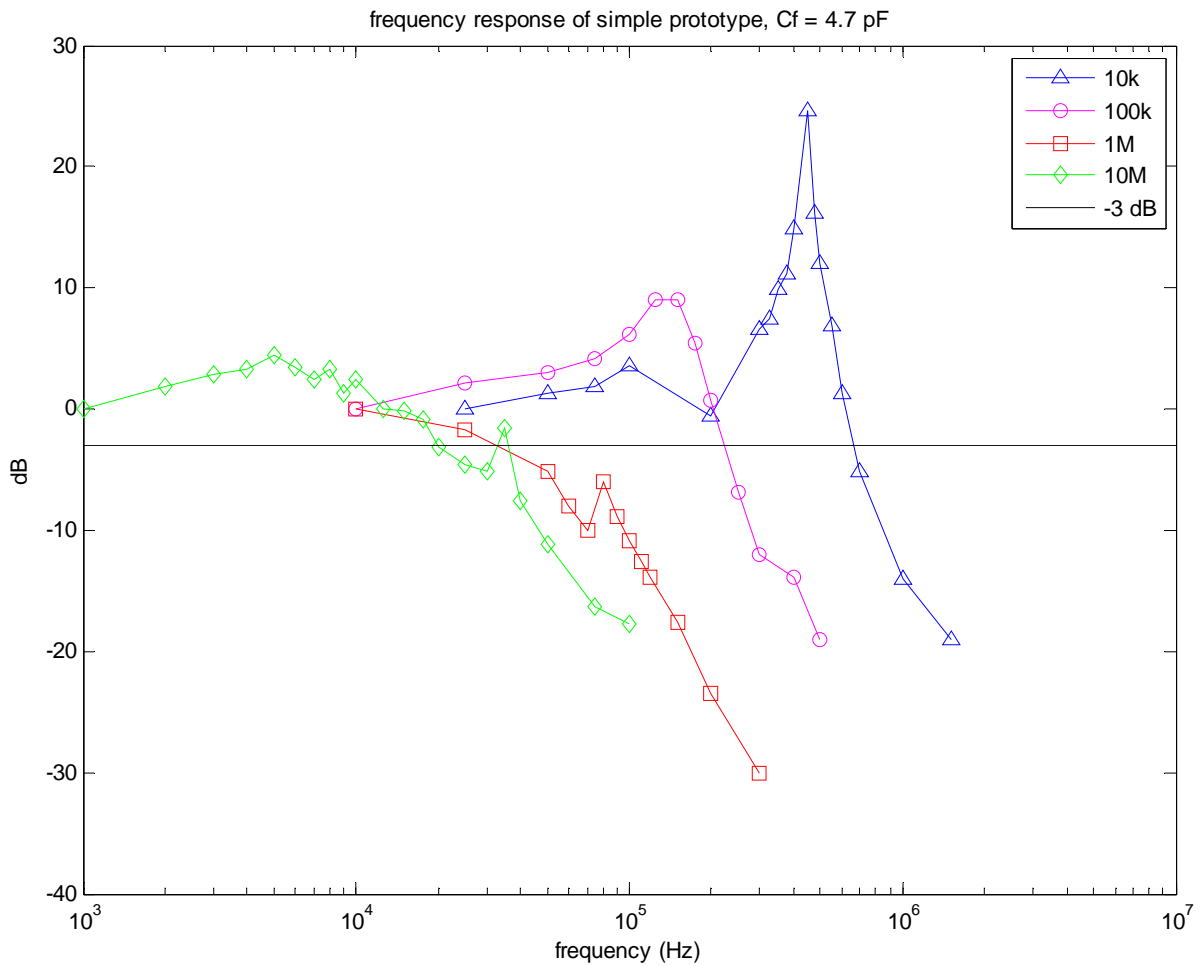
The photodiode showed a very uniform responsivity in the x direction (moving parallel to the base of the photodiode with the wire outputs). The largest variation in the x direction was 0.5%. In the y direction, the responsivity increased slightly as the beam became closer to the wire outputs. The largest variation in the y direction was 2.5%.

2.5.2 First Iteration Simple Prototype

The first iteration of the simple prototype performed reliably and predictably. The frequency response of the circuit for each of the four gain stages is shown in Figure 12. The resonant peaks in each of the curves are a result of a similar resonance present in the frequency response of the OPA381 op amp^[4]. These peaks are present at some level in all of the frequency response curves for circuits that include the OPA380 or OPA381.



(a)



(b)

Figure 12 Simple prototype basic circuit (a) and first iteration frequency response, $C_F = 4.7 \text{ pF}$ (b). The resonant peaks seen in this and following frequency responses are a direct result of resonant peaks in the OPA380^[4] and OPA381^[19] closed loop gain curves.

After a brief qualitative power calibration to learn the rough range of the photodiode sensitivity, it was determined that the circuit response was roughly linear from 0 to roughly 4.4 V, just below the positive rail for the OPA381 when it is powered on the positive supply by 5 V. It was also determined that the 10 k Ω gain stage would be unnecessary because the upper optical power of interest specified in the project objectives (10 μ W) was easily covered by higher gain stages. Also, to improve the signal noise ratio at the low end of the optical power of interest (10 nW), a higher gain resistor of 100 M Ω was added to future prototypes.

The noise at each relevant gain stage is shown in Table 1. There was a strong harmonic present at roughly 270 Hz, which remained unexplained.

Gain	RMS Voltage Noise
100 kΩ	2.5 mV
1 MΩ	3 mV
10 MΩ	4 mV

Table 1 Simple prototype first iteration RMS noise, $C_F = 4.7$ pF.

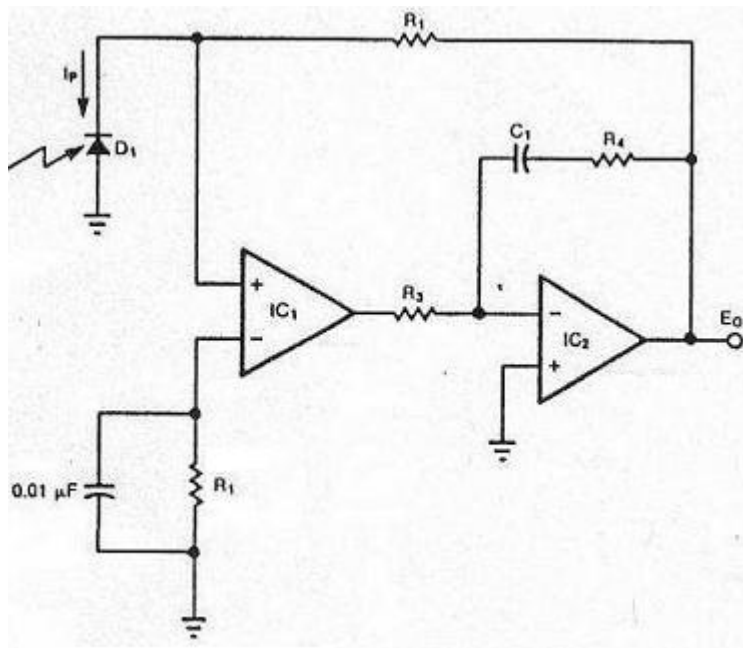
Qualitative testing with the feedback capacitor removed (some feedback capacitance will remain due to the stray capacitance associated with the feedback resistor and circuit board) showed the expected results. The bandwidth increased significantly – from roughly 20 kHz to roughly 60 kHz at 10 M Ω gain – but the noise also increased significantly, going from 4 mV RMS to about 20 mV RMS.

Biasing the photodiode in this circuit did not improve the noise performance; in fact, it weakened it. Due to an error in the biasing scheme design, the biasing was achieved by shorting the photodiode cathode to the -5 V power supply input line. One possible explanation considered for the poor performance with this biasing scheme was that the bias voltage was unregulated, and potentially noisy. To test this, the biasing design error was updated in the second iteration; however, biasing the photodiode still did not improve the noise performance for the simple design.

2.5.3 First Iteration Two Stage Prototype

Initial testing of the two stage prototype with no bias voltage applied to the photodiode showed stable operation in the higher gain stages, but the circuit oscillated rail to rail in the 100 k Ω gain stage. Applying a -5 V bias voltage improved the performance of all stages, and allowed stable operation at 100 k Ω . Quick tests of bandwidth with and without bias demonstrated that the frequency response of the circuit was unaffected by bias voltage, as expected. Because the two stage prototype showed occasional instability, a larger feedback capacitor of 10 pF was used for testing to help reduce the possibility of instability by reducing noise gain, which can initiate oscillation.

The frequency response for the two stage prototype is shown in Figure 13. The frequency response was measured with no bias voltage for the 1 M Ω and 10 M Ω stages, but to avoid oscillation and allow for testing, with a -5 V bias applied for the 100 k Ω stage.



(a)

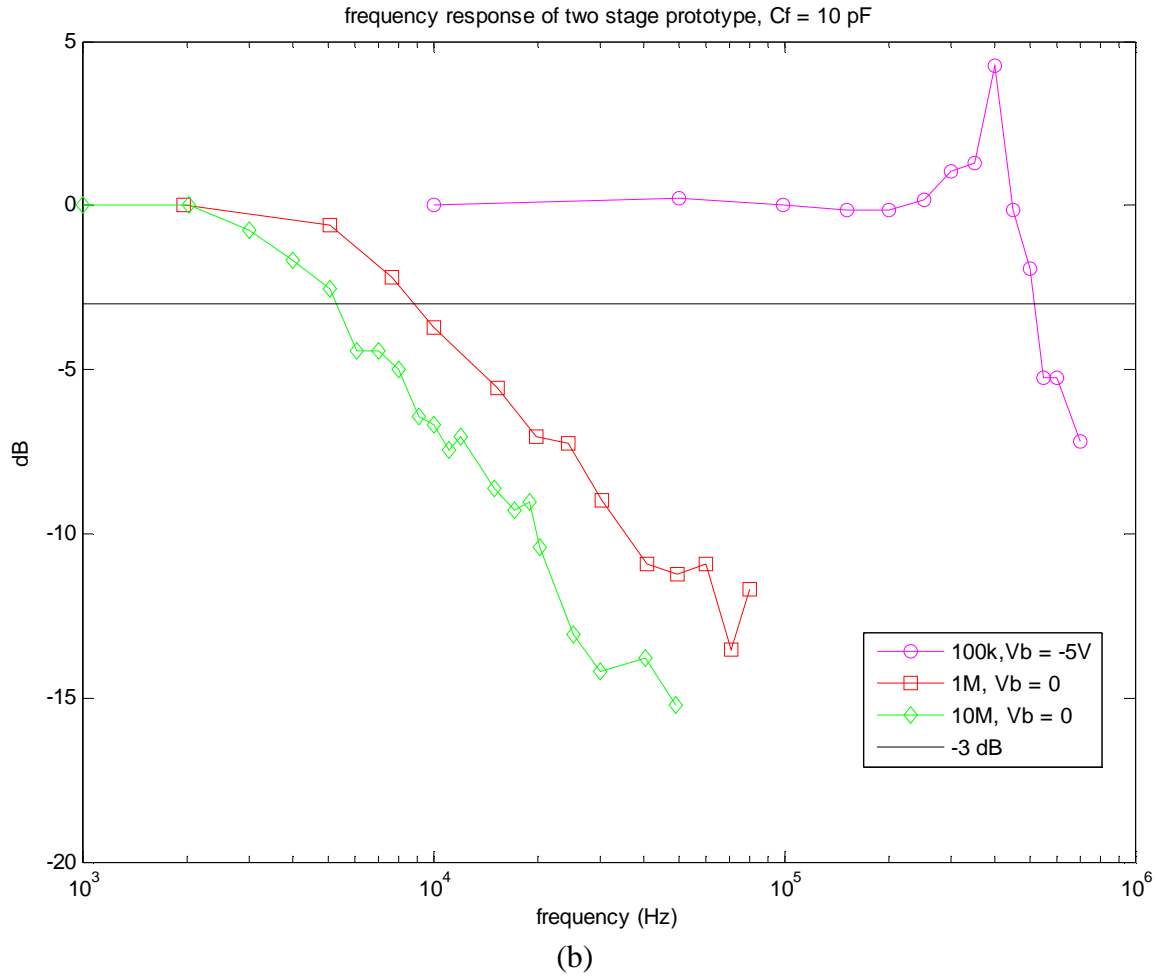


Figure 13 Two stage prototype basic schematic (a) and first iteration frequency response with $C_f = 10 \text{ pF}$ (b).

Aside from allowing stable operation in the $100 \text{ k}\Omega$ gain stage, applying bias voltage to the photodiode improved the noise performance of the circuit, and caused a dark current to be emitted from the photodiode, leading to an output voltage on the detector even when no input signal is present on the photodiode. This dark output was negligible at low gain, but when amplified more strongly in the higher gain stages, became significant. The dark output at each of the gain stages is shown in Table 2.

Gain	Dark Output
100 k Ω	< 5 mV
1 M Ω	20 mV
10 M Ω	200 mV
100 M Ω	1.92 V

Table 2 Two stage prototype dark current output with -5 V bias on photodiode

The dark current is particularly problematic at the 100 M Ω gain stage, where it removes nearly half of the dynamic range of the op amp.

The noise in the circuit both with and without bias voltage is shown in Table 3.

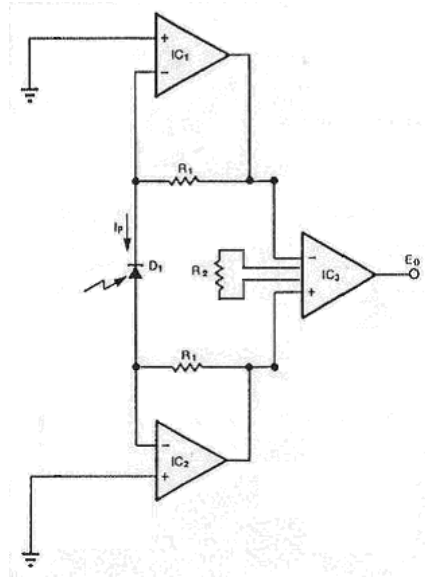
Gain	Bias Voltage	RMS Voltage Noise
100 k Ω	0 V	Oscillating
100 k Ω	-5 V	1.5 mV
1 M Ω	0 V	4.5 mV
1 M Ω	-5 V	2.5 mV
10 M Ω	0 V	5 mV
10 M Ω	-5 V	2.5 mV
100 M Ω	0 V	5 mV
100 M Ω	-5 V	4.5 mV

Table 3 Two stage prototype first iteration RMS noise, $C_F = 10$ pF.

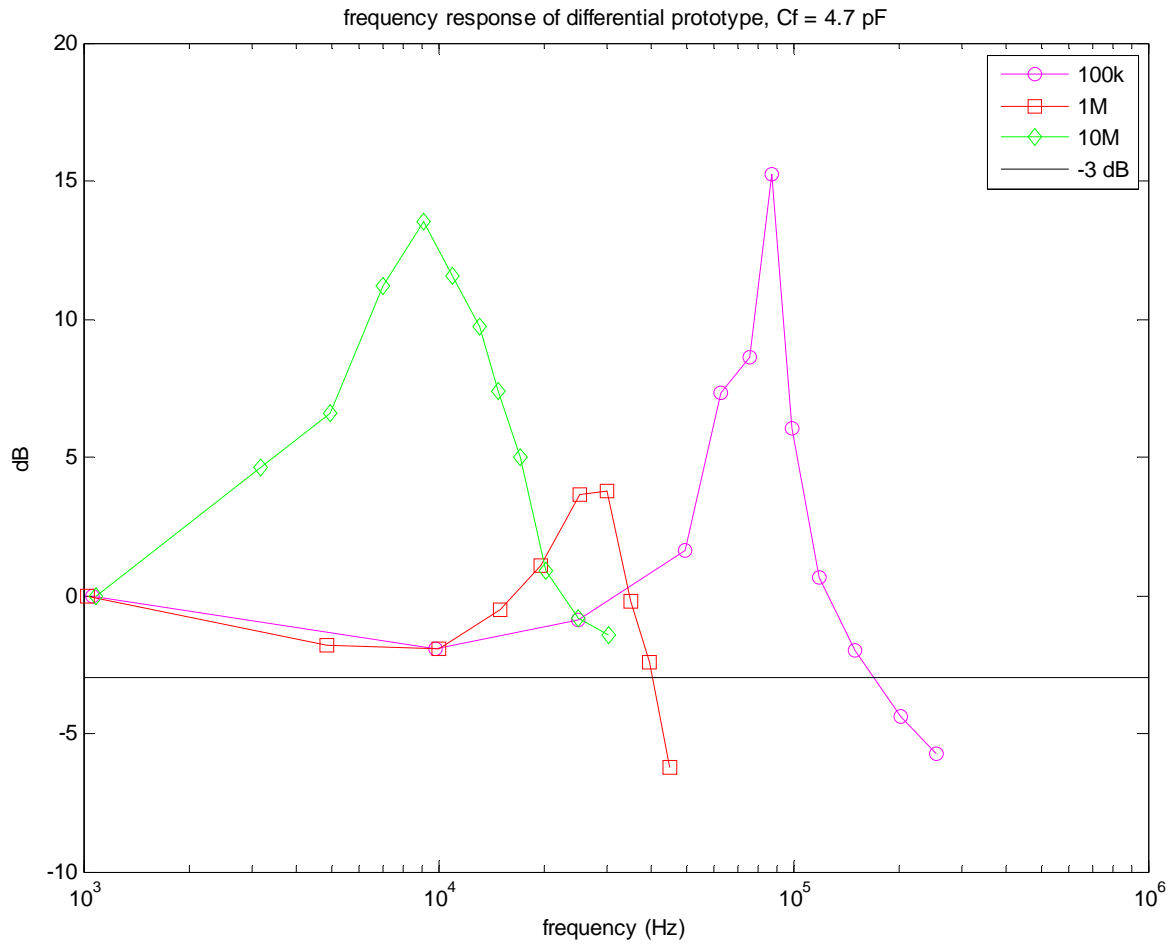
The circuit had some glitches. Oscillation without bias voltage occurred always in the 100 k Ω gain stage, and with smaller feedback capacitors, also occurred sporadically in other gain stages. Also, the output of the circuit occasionally jumped to the positive rail. The circuit performed well from a noise and bandwidth perspective, but showed some unreliability. In an effort to improve this, the second iteration was tweaked and the op amps replaced.

2.5.4 Differential Prototype

The differential based prototype performed very reliably, but did not meet expectations in noise performance. The frequency response of each gain stage is shown in Figure 14.



(a)



(b)

Figure 14 Differential prototype basic schematic (a) and frequency response with $C_F = 4.7 \text{ pF}$ (b).

The bandwidth is not significantly different than the other circuits, but the noise performance, summarized in Table 4, was considerably worse. In particular, the main attraction of the differential design – the use of a high common mode rejection ratio instrumentation amplifier for eliminating power supply and other common noise – was ineffective. Power supply noise was still clearly present.

Gain	RMS Voltage Noise
100 kΩ	4 mV
1 MΩ	6 mV
10 MΩ	7 mV
100 MΩ	9 mV

Table 4 Differential prototype RMS noise, $C_F = 4.7$ pF

2.5.5 Second Design Iteration

The second iteration of prototypes included new versions of the simple prototype and the two stage prototype, as well as a new design: the bootstrapped cascode.

The performance of the second simple prototype is summarized by Table 5. Bias voltage applied to the photodiode again showed no improvements. The noise and bandwidth are both larger than the first prototype, but this is due to the fact that the measurements were done with no feedback capacitor. The simple prototype again performed very reliably.

Gain	3 dB Bandwidth	RMS Voltage Noise
100 kΩ	150 kHz	4 mV
1 MΩ	80 kHz	6 mV
10 MΩ	22 kHz	9 mV
100 MΩ	10 kHz	13 mV

Table 5 Simple prototype second iteration results, $C_F = 0$

The second version of the two stage prototype performed very erratically. Oscillation in all gain stages both with and without bias randomly occurred for unidentifiable reasons,

and the circuit output often railed at the positive op amp supply. When the circuit worked, it performed similarly to the first iteration.

The last prototype, the bootstrapped cascode, showed very good noise performance at low gain, but was permanently saturated at all gains higher than 100 k Ω . This is due to the fact that the “bootstrapping” part of the circuit, which linearizes the transistor Q1 of Figure 9 by supplying a small bias current to the base, supplies a current that is large enough to saturate the amplifier without any photocurrent.

2.5.6 Final Design Selection

Based on the results of the first design iteration, the differential amplifier was abandoned due to poor noise performance, and the simple and two stage designs were carried through to a second, tweaked design. The goal was to improve the reliability of the two stage design, make small tweaks to the simple design for further testing, and investigate the bootstrapped cascode design. The bootstrapped cascode could potentially be tweaked to be suitable for the intended application, but due to the complexity of the circuit and limited time frame for completion, immediately reliable operation was deemed paramount.

The selection between the simple prototype and the two stage design was made based on the same philosophy. The two stage amplifier could likely be tweaked and tested to the point of providing a detector with the same reliability as the simple design, and based on the idea of the circuit and the test results from the first iteration, likely perform at a higher level. However, given the time constraints and necessity of producing a working final product, as well as the fact that the simple prototype performed very reliably at a level very close to meeting all of the project objectives, the two stage design was dropped in favour of the simple design.

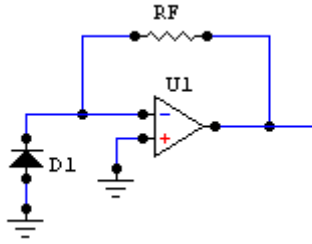


Figure 15 Final design basic schematic. The simple transimpedance amplifier performed most reliably.

2.5.7 Final Circuit, 1 pF Feedback Capacitance

The final circuit was professionally fabricated by Canadian Circuits. The schematic and PCB layout are shown in Appendix B. For baseline testing, the circuit was characterized fully with a 1 pF capacitor. Also, to best achieve the project objectives, a new set of gain resistors was chosen: 1 M Ω , 10 M Ω , 50 M Ω , and 100 M Ω . The motivation for the new choices was to provide the ability for very low noise, high sensitivity DC measurements in which bandwidth is not a concern, while still allowing for the possibility of faster high sensitivity measurements where some noise performance is sacrificed.

The frequency response of the final circuit with a 1 pF feedback capacitor and the OPA380 is shown in Figure 16.

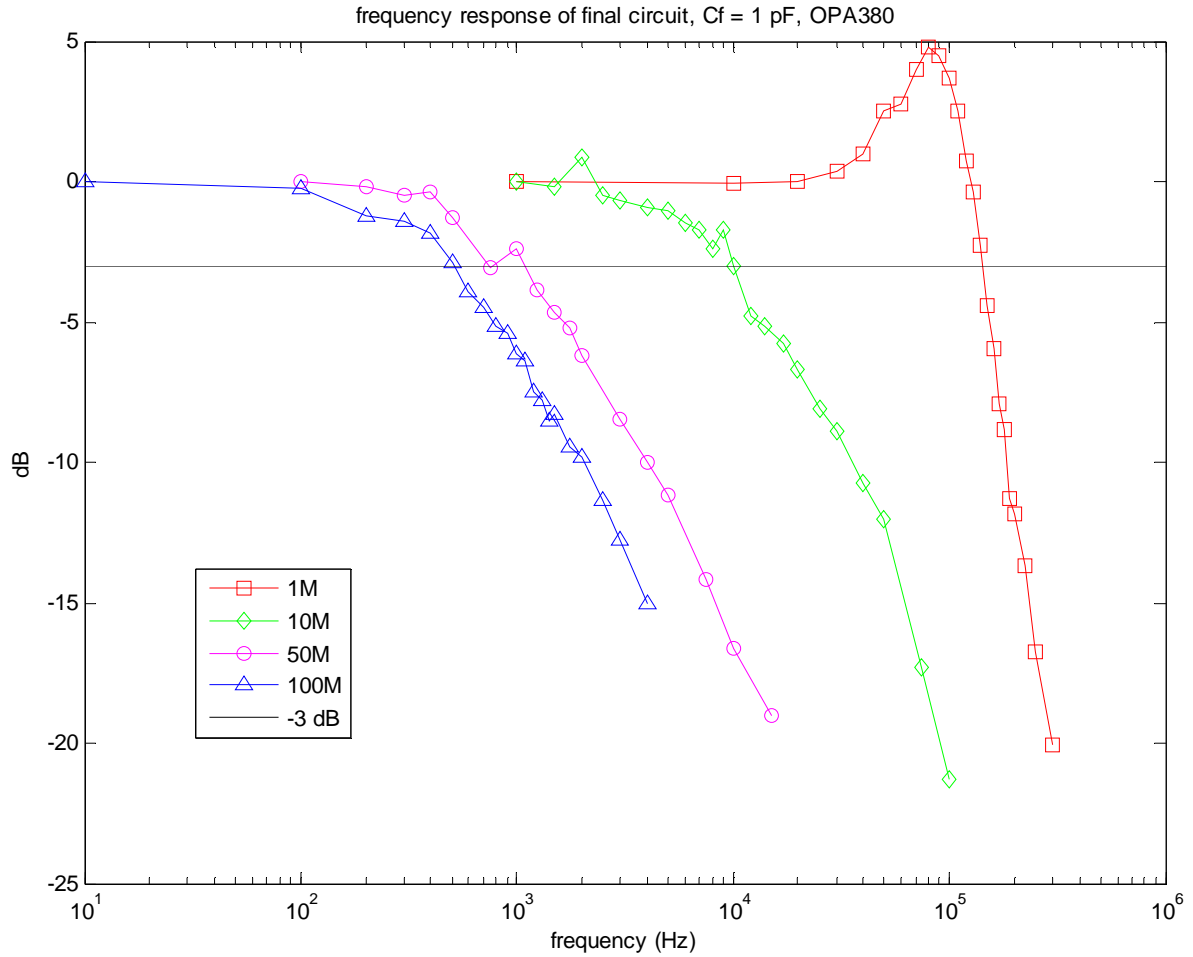


Figure 16 Final circuit frequency response, OPA380, $C_F = 1$ pF.

The noise performance was once again tested both with and without bias voltage applied to the photodiode. The circuit was also tested with both the OPA380 and OPA381 for direct comparison. The results are summarized in Table 6.

Gain	Bias Voltage	RMS Voltage Noise (OPA380)	RMS Voltage Noise (OPA381)
1 M Ω	0 V	7.4 mV	5.2 mV
1 M Ω	-5 V	7.2 mV	-
10 M Ω	0 V	12 mV	8.6 mV
10 M Ω	-5 V	21 mV	-
50 M Ω	0 V	16 mV	9.6 mV
50 M Ω	-5 V	27 mV	-
100 M Ω	0 V	23 mV	10 mV
100 M Ω	-5 V	29 mV	-

Table 6 Final circuit comparison of RMS noise levels, $C_F = 1$ pF.

The noise performance is clearly better with the OPA381, as anticipated. This is due to the restricted bandwidth of the OPA381 in comparison with the OPA380. Because the signal bandwidth is limited by the feedback resistor and capacitor combination, and not the op amp gain bandwidth product (GBW), the excess bandwidth provided by the OPA380 (90 MHz GBW compared to 18 MHz GBW) is not useful for amplifying signal. It does, however, amplify the high frequency band of op amp noise in accordance to the ratio of the feedback capacitance and the photodiode capacitance. The result is worse noise performance with no bandwidth improvement. The frequency response of the circuit with the OPA380 and OPA381 were measured to be the same, as expected.

Also, the OPA380 does not pull its output all the way to the negative supply rail (ground). Useful, linear output begins at roughly 50 mV. The OPA381, however, pulls the output to ground and shows a linear response from the negative rail almost all the way to the positive rail at about 4.4 V.

The final circuit was also tested with various feedback capacitors to determine the optimal feedback capacitor for each gain resistor. The results are shown in Table 7.

Feedback Capacitance	1 MΩ RMS Voltage Noise	10 MΩ RMS Voltage Noise	50 MΩ RMS Voltage Noise	100 MΩ RMS Voltage Noise
470 pF	760 μV	750 μV	800 μV	850 μV
47 pF	1 mV	950 μV	1.1 mV	1 mV
10 pF	1.7 mV	2.2 mV	2.3 mV	2.5 mV
4.7 pF	2.5 mV	3.8 mV	4.1 mV	4.1 mV
2.7 pF	3.5 mV	5.4 mV	5.8 mV	6 mV

Table 7 Final circuit noise comparison with different feedback capacitors, OPA381.

2.5.8 Final Photodetector

The final photodetector uses no bias voltage, an OPA381 op amp, and feedback capacitors suited for the intended function of each gain stage. The feedback capacitor for

each gain stage and the rotary switch position to select the desired gain stage are shown in Table 8.

Gain	Feedback Capacitance	Switch Position
1 M Ω	10 pF	1
10 M Ω	2.7 pF	2
50 M Ω	1 pF	3
100 M Ω	47 pF	4

Table 8 Final detector gain resistances, feedback capacitances, and switch positions

The frequency response of the final photodetector in its final configuration is shown in Figure 17.

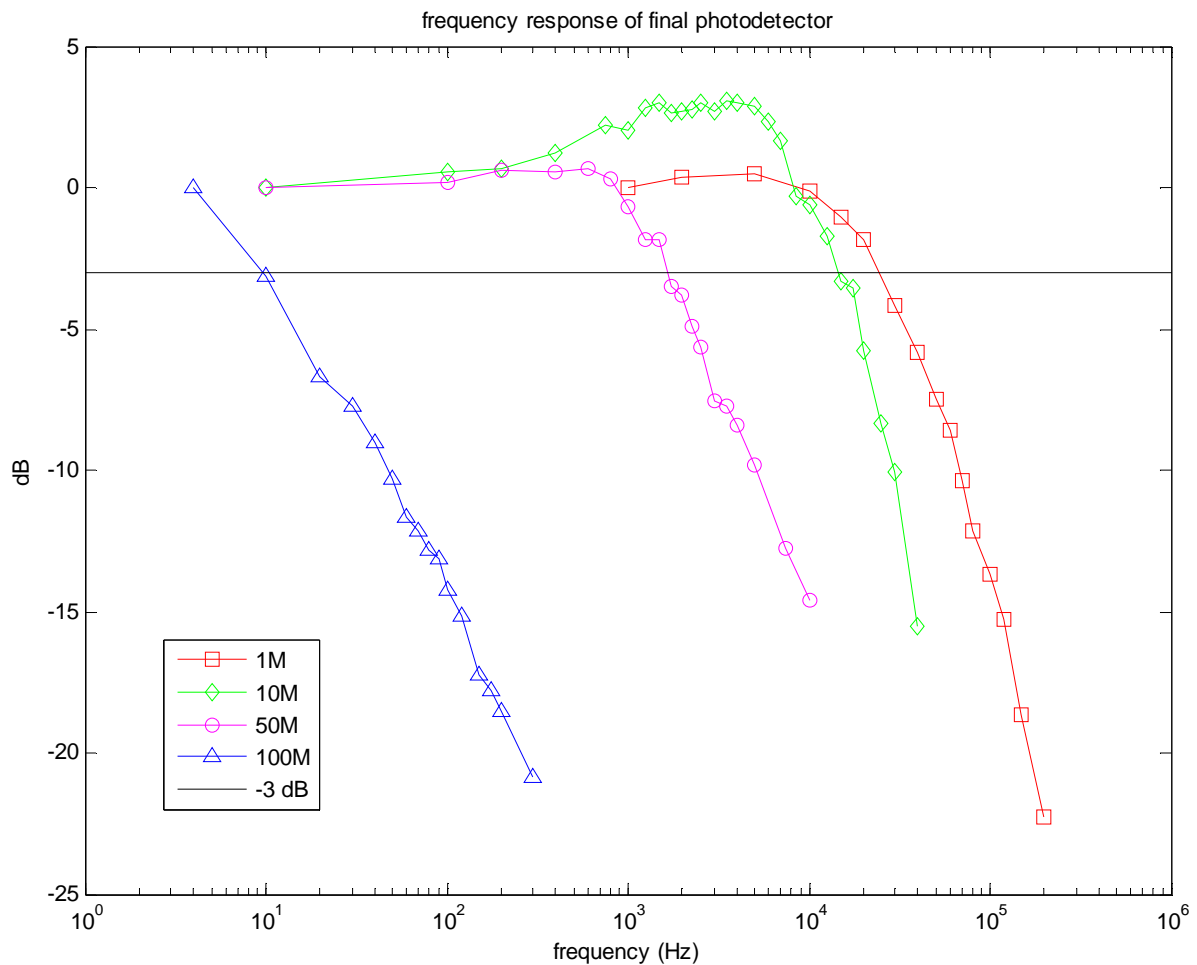


Figure 17 Final detector frequency response. The 100 M Ω gain stage is intended for high precision DC measurements, while the 50 M Ω gain stage is intended to be a high speed high sensitivity setting that sacrifices noise performance.

Table 9 summarizes the key performance metrics of the final photodetector.

Gain	3 dB Bandwidth	RMS Voltage Noise
1 MΩ	60 kHz	1.8 mV
10 MΩ	17 kHz	5.0 mV
50 MΩ	2.5 kHz	8.0 mV
100 MΩ	~10 Hz	1.0 mV

Table 9 Final detector bandwidth and noise summary.

The feedback capacitors were selected to optimize each gain stage. The 1 M Ω and 10 M Ω gain stages are general purpose, optimized for a combination of good noise performance and high bandwidth. The 50 M Ω gain stage is intended to be a high sensitivity setting that provides enough bandwidth for reliable measurement stability on the millisecond scale while maintaining a reasonable noise level. The 100 M Ω gain is intended to be a setting used for DC measurement only, providing very high sensitivity and excellent noise performance. Tweaking the capacitors further can alter the noise/bandwidth trade-off to whatever is desirable, without affecting the power calibration.

The input power to output voltage calibration for the first completed detector, labelled Detector 2, is shown in Figures 18 through 21. Linearity is achieved in all gain stages from the negative rail up to near the positive rail.

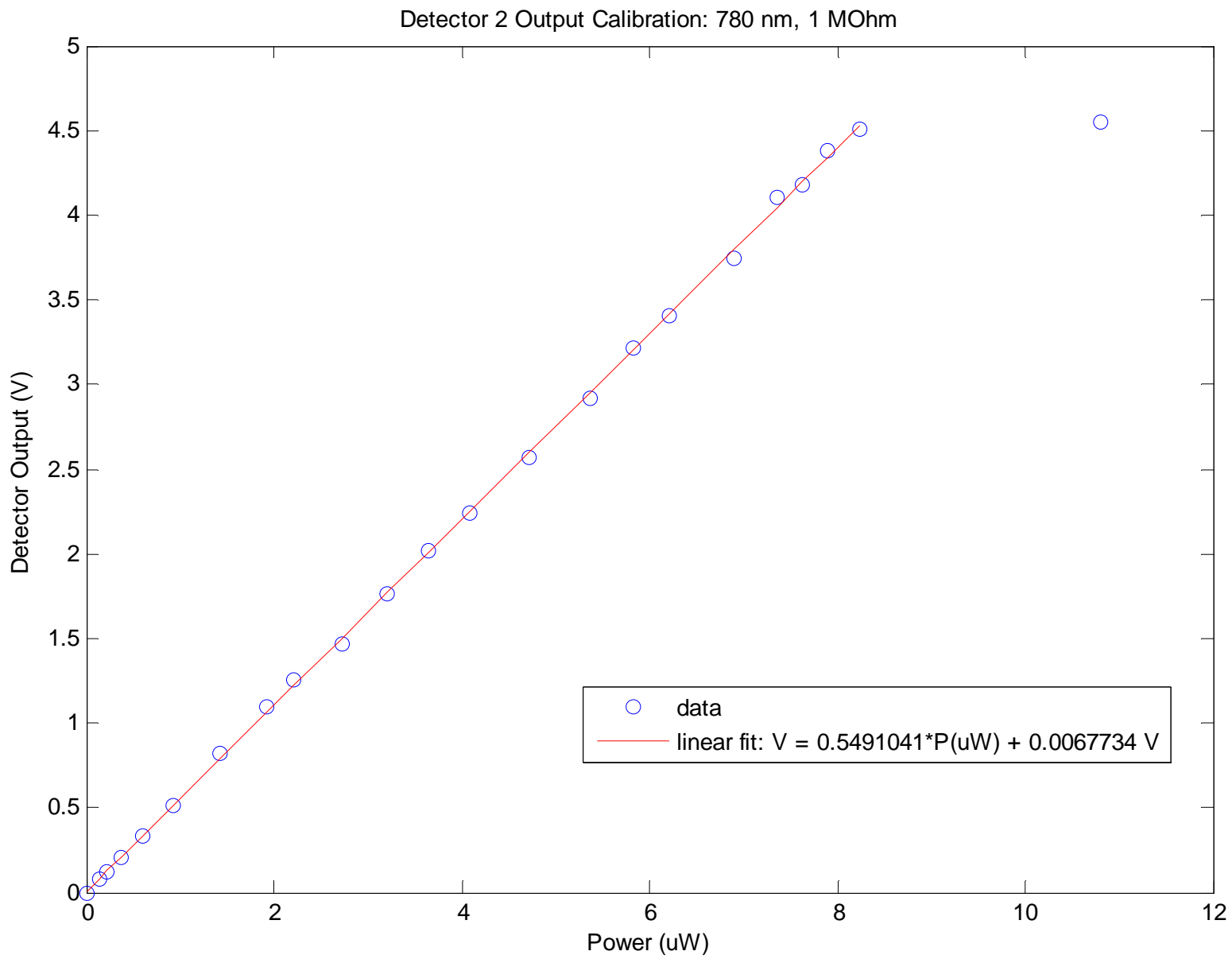


Figure 18 Power calibration curve for Detector 2, 780 nm, 1 MΩ gain.

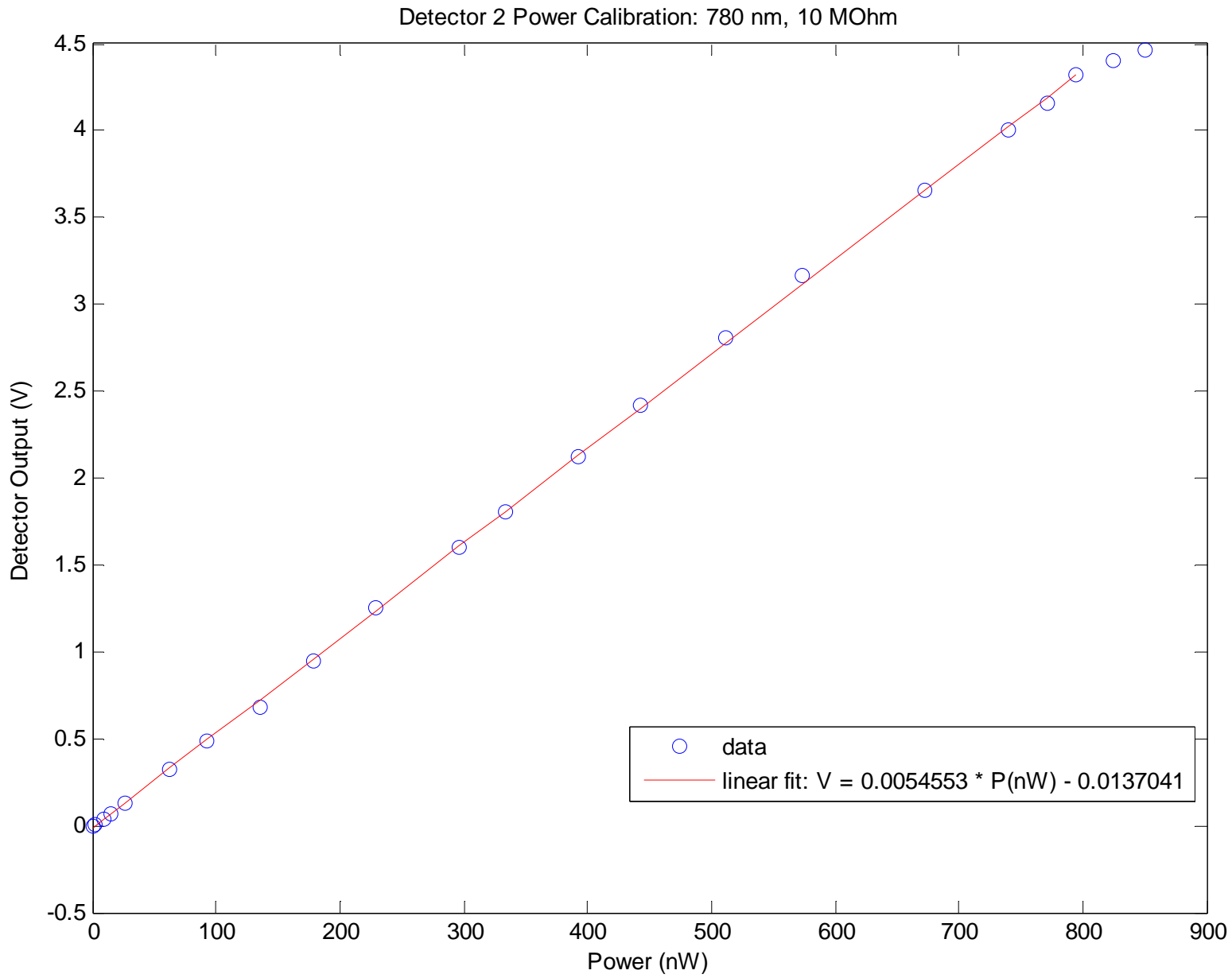


Figure 19 Power calibration curve for Detector 2, 780 nm, 10 MΩ gain.

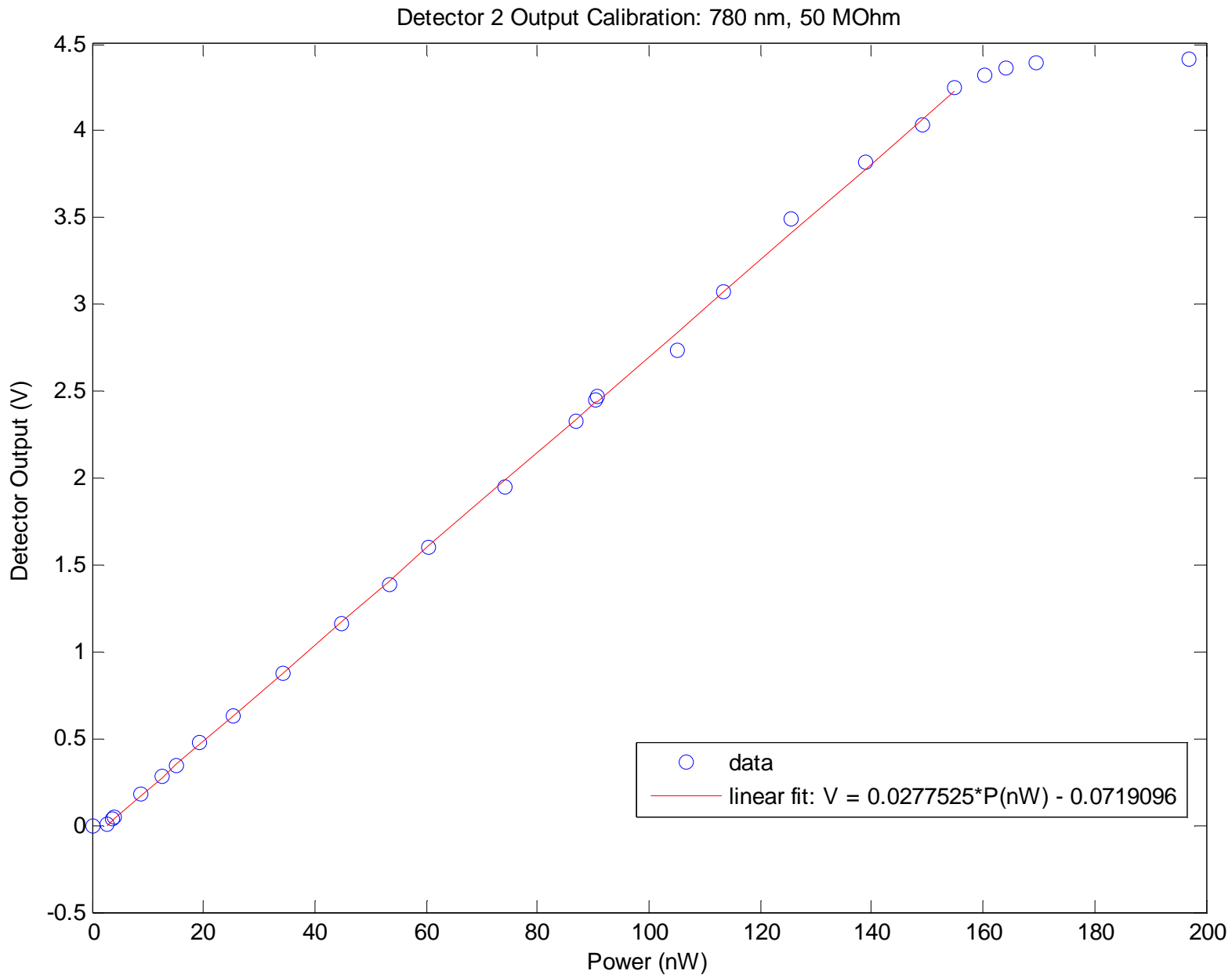


Figure 20 Power calibration curve for Detector 2, 780 nm, 50 MΩ gain.

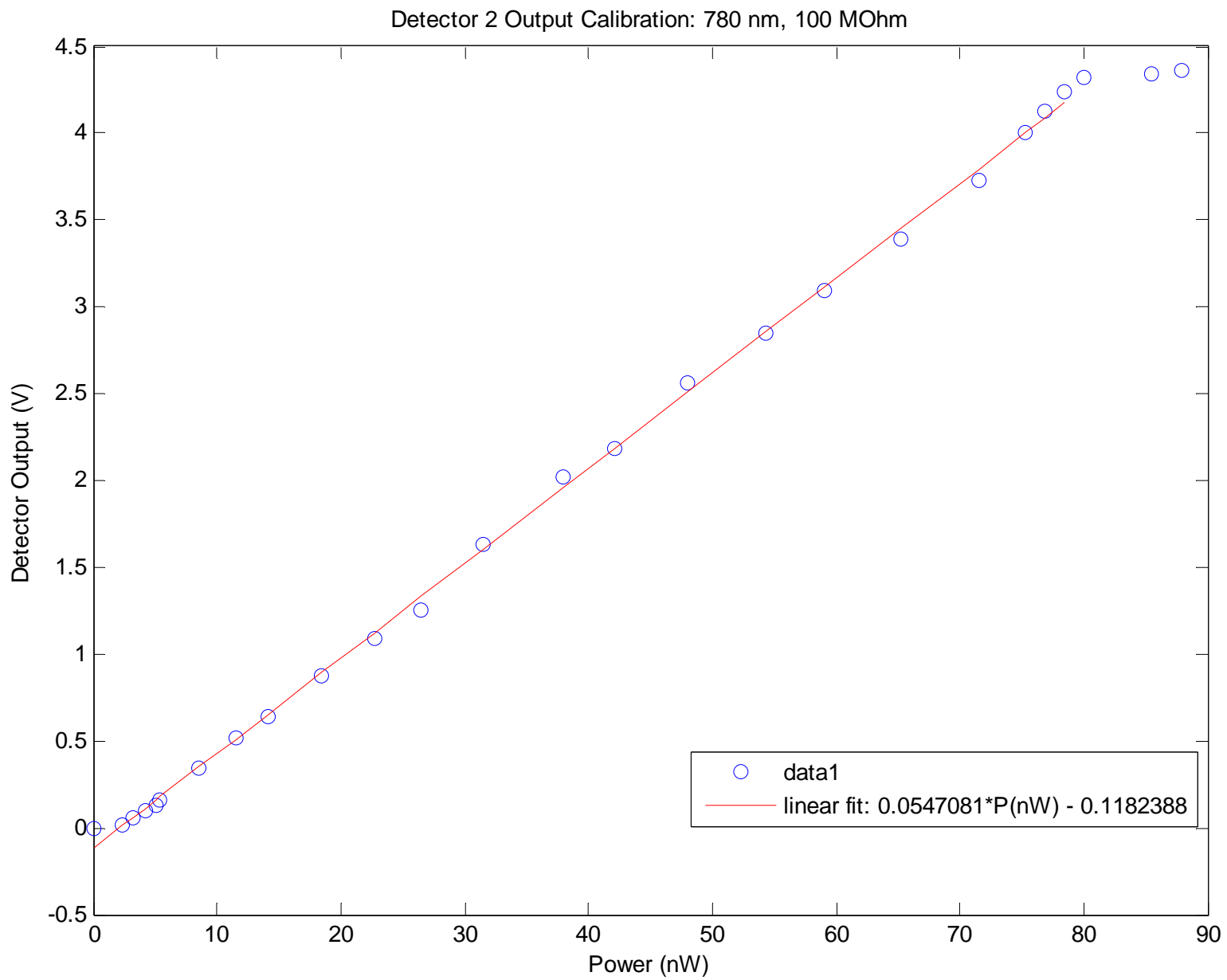


Figure 21 Power calibration curve for Detector 2, 780 nm, 100 MΩ gain.

The signal to noise ratio (SNR) is well above the target specification of 40 dB for the majority of the power detection range specified in the project objectives (10 nW to 10 μ W). The SNR at the minimum power of interest, 10 nW, is roughly 53 dB. The lowest values of SNR in the detection range of interest occur when the detector is operated in a region where the amplifier output is in the low portion of its full output scale. These necessarily occur at boundaries between gain stages where the higher gain saturates and the next lower gain stage must be used. The boundary between 100 M Ω and 50 M Ω occurs at roughly 80 nW; the SNR in the 50 M Ω stage at 80 nW is roughly 48 dB. The boundary between 50 M Ω and 10 M Ω occurs at roughly 155 nW; the SNR in the 10 M Ω stage at 155 nW is roughly 43 dB. The boundary between 10 M Ω and 1 M Ω occurs at roughly 780 nW; the SNR in the 1 M Ω stage at 780 nW is roughly 44 dB. Thus, the minimum signal to noise ratio of the detector through the power range of interest is 43 dB, and the SNR is normally much higher. However, in the highest gain stage, the bandwidth is very limited. For fast, high sensitivity measurements, the 50 M Ω gain stage must be used. At 10 nW, the SNR is roughly 30 dB.

3 Conclusions

Prior to completion, the project went through various stages. First, a set of initial prototypes were designed and fabricated. Following this, each prototype was tested and characterized for comparison, and after evaluation of these results, a second round of prototypes was issued. Following the characterization of this second iteration design set, a basic transimpedance amplifier design was selected for the final application based on test results which showed competitive performance in noise and bandwidth and extremely high reliability. Design, PCB layout, and fabrication of the final circuit took place in conjunction with a mechanical design encompassing the housing and integration of the detectors into existing optical systems. Finally, the final circuits were populated, tested, characterized, and calibrated, before being placed into the systems for which they were designed.

The final product in large part met the objectives specified at the outset of the project. The noise performance achieved was good, with noise levels measured at 1.8 mV RMS for the 1 M Ω gain stage, 5 mV RMS for the 10 M Ω gain stage, 8 mV RMS for the 50 M Ω gain stage, and 1 mV RMS for the 100 M Ω gain stage. The noise performance for each gain stage was defined largely by the combination of the feedback resistance and capacitance; better noise performance was achieved in the 100 M Ω gain stage than the 50 M Ω gain stage by including a larger feedback capacitor, although this sacrifices significant bandwidth. The minimum signal to noise ratio (SNR) throughout the detection range was 43 dB, clearing the objective of 40 dB. The optimal SNR at the lowest power of interest, 10 nW, was 57 dB, and the SNR throughout the majority of the detection range is above 60 dB, achieving a maximum of 73 dB. The detector is able to meaningfully read powers below 1 nW, exceeding the range of power required, although at 1 nW the SNR is only 37 dB. The sensitivity and adjustable gain targets were met and exceeded.

The bandwidth target was only partially achieved. Due to the high noise resulting from the very large photodiode capacitance and high gain required to achieve the desired

sensitivity, the bandwidth specification proved difficult to meet without completely sacrificing noise performance. At the two lower gain stages, 1 M Ω and 10 M Ω , the bandwidth specification was exceeded, with 3 dB bandwidths of 60 and 17 kHz, respectively. However, at the higher gain stages, the bandwidth and noise trade-off suffered. As a compromise solution, two high sensitivity gain stages were provided: a 100 M Ω stage with very low bandwidth (~10 Hz) but very low noise for high precision slow measurements, and a 50 M Ω stage with higher bandwidth (2.5 kHz) and higher noise for less precise faster measurements. Although 2.5 kHz does not meet the 10 kHz bandwidth target, it still allows measurement rise and fall times fast enough to be stable within one millisecond. The minimum signal to noise ratio in this stage, occurring at the minimum power of interest, 10 nW, falls slightly short of the 40 dB specification at 36 dB. Thus, the objective specifications are not simultaneously met throughout the entire detection range, but are met for the large majority of the detection range.

The final detectors employ large area 1 cm² FDS1010 photodiodes ^[20], allowing easy alignment even at the very low optical power expected. The detectors were also calibrated for 780 nm and 671 nm. The final product includes a compact housing, combined with optical mounts allowing easy implementation into any optical system, an iris and filter built on, and the desired BNC output and standard lab power supply connection interface.

4 Recommendations

Although the photodetectors are complete and form a final product that will not be altered, recommendations can be made about how to proceed with implementing them into optical systems and how to potentially improve the design for future projects.

Isolating optical noise from the signal using bandpass filters should be more closely investigated. Because the bandpass filters attenuate strongly even at the pass frequency, the sensitivity and signal to noise ratio will be negatively affected. More importantly, bandpass filters show alignment sensitivity that would impact the calibration factor dependent on the orientation. Lens tubes may be a more effective means of isolating optical noise.

If improvements to the design are desired for future work, the authors recommend investing further time in the two stage circuit (Figure 6) and the bootstrapped cascode (Figure 9). The two stage circuit would likely require testing more op amps, tweaking component values, and identifying conditions leading to oscillation. The bootstrapped cascode circuit could also potentially exceed the performance of the design used in this project, but would likely require much more effort to achieve the performance. Finding transistors which have very low operating currents would be helpful in eliminating the problem of the bias current overrunning the signal current.

For simple adjustments to the bandwidth/noise trade-off, the feedback capacitors for each gain resistor can be replaced with different value capacitors as necessary. In the final schematic and PCB layout of Figures 28 and 29, respectively, these capacitors are labelled C2, C3, C8, and C9. Adjusting the capacitor to a higher value will result in improved noise performance, but decreased bandwidth, and vice versa.

Appendix A: Prototype Schematics

Schematics from all of the prototypes tested are included below.

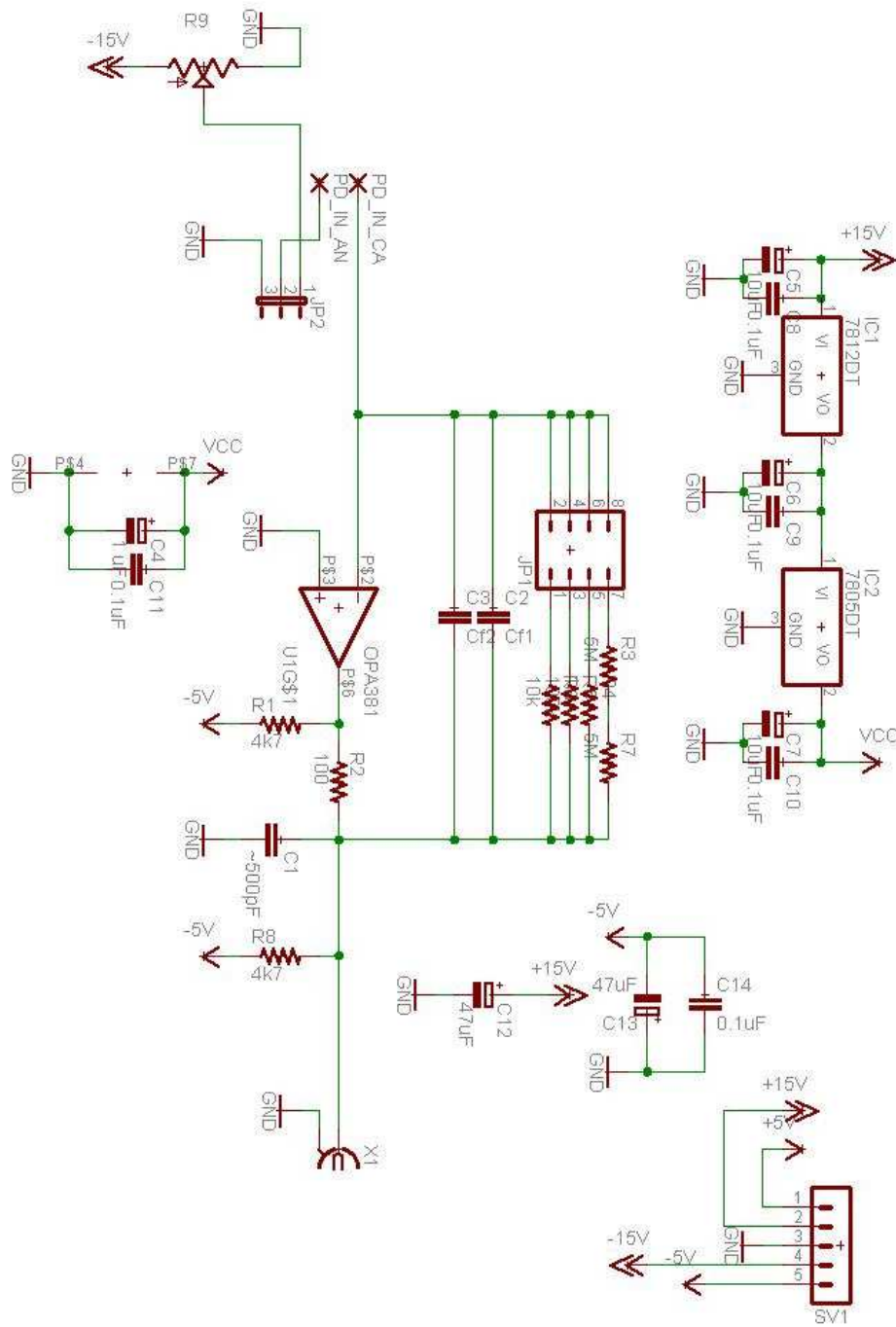


Figure 22 Simple prototype first iteration schematic.

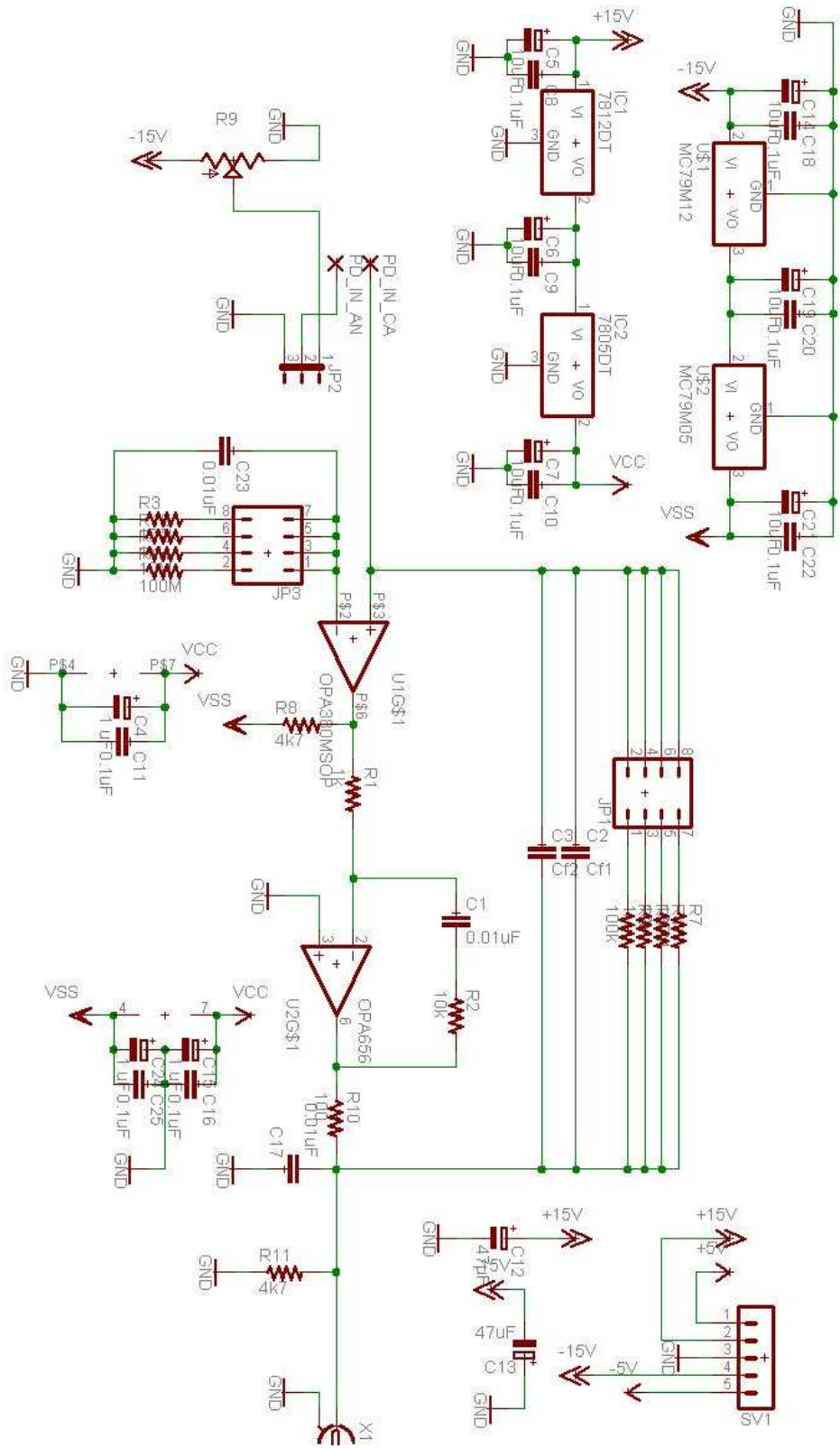


Figure 23 Two stage prototype first iteration schematic.

In the first iteration simple and two stage designs, the bias voltage scheme contains an error. Potentiometer R9 in both schematics sets the bias voltage through a jumper allowing the user to choose a bias voltage set by R9 or ground. The wiper of the potentiometer should in both cases be buffered before connecting to the jumper. This error is corrected in the second iteration of both designs.

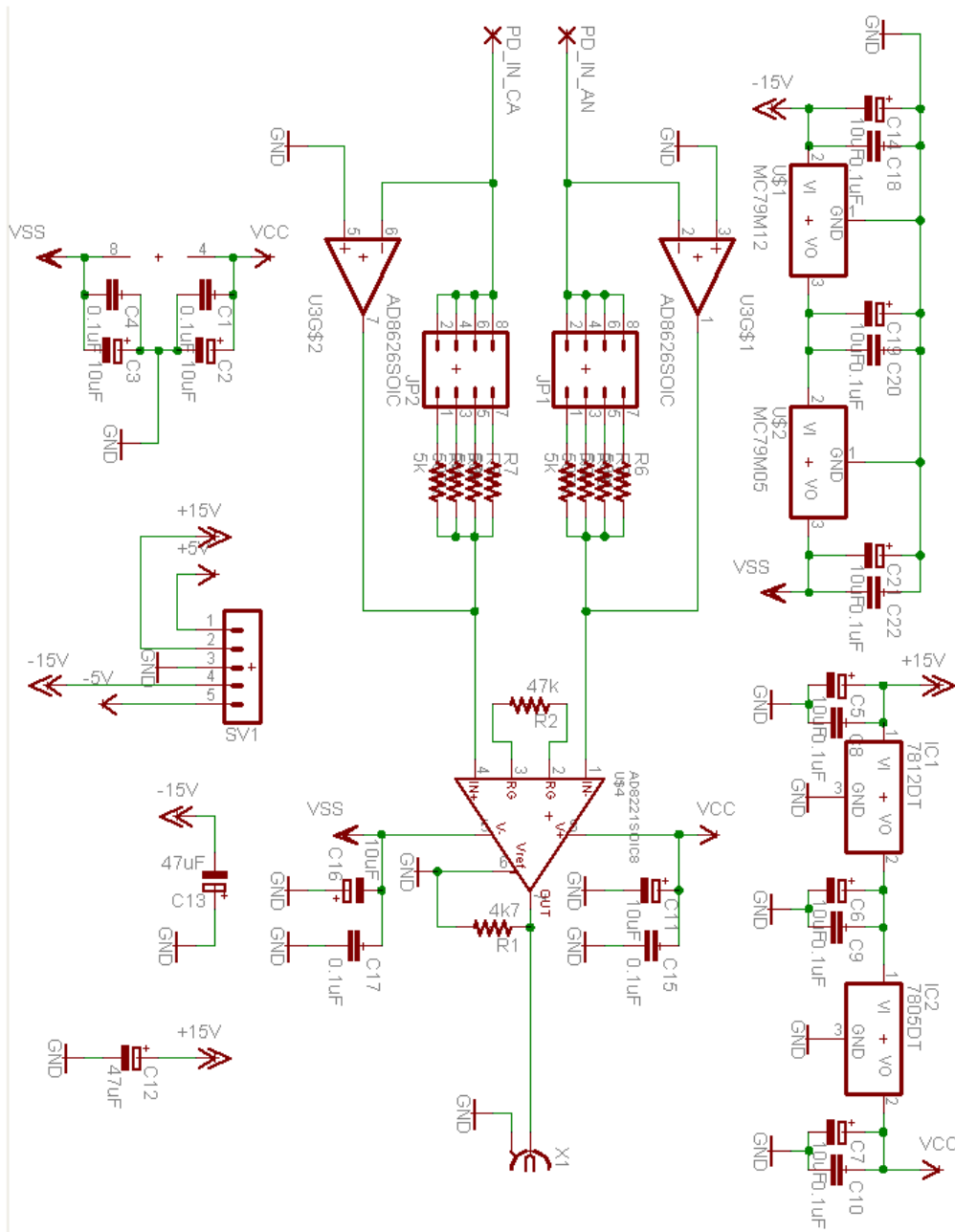


Figure 24 Differential prototype schematic.

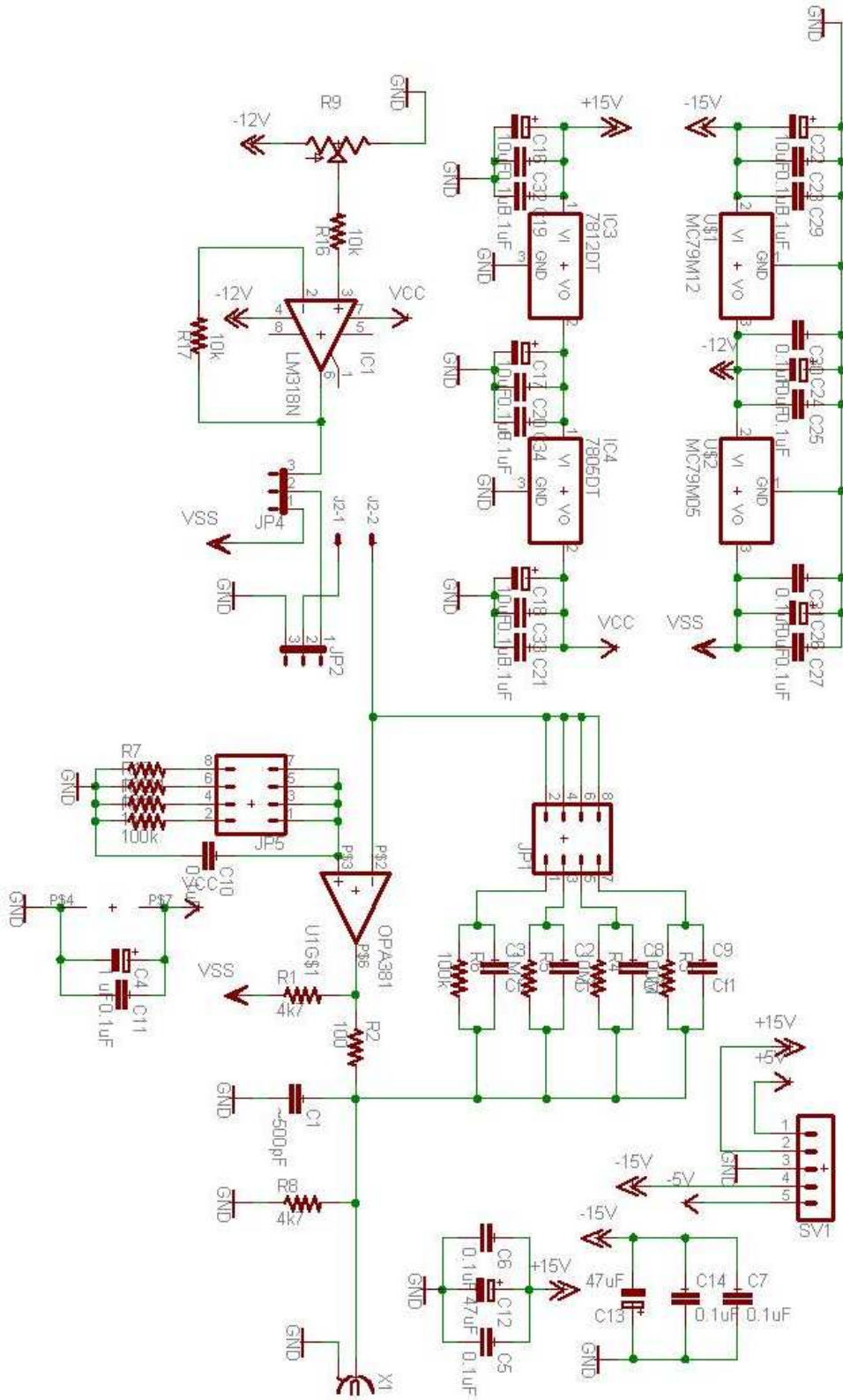


Figure 25 Simple prototype second iteration schematic.

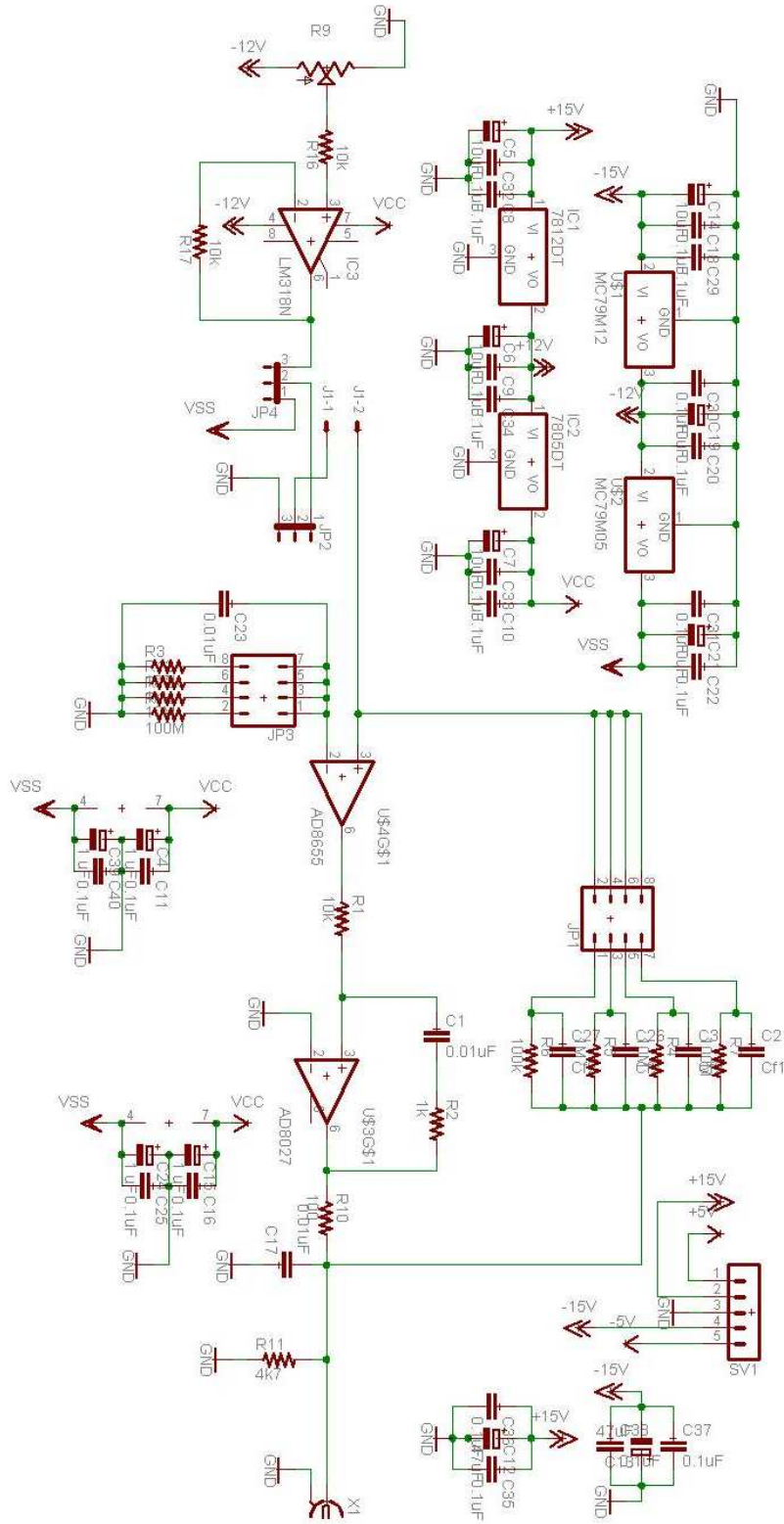


Figure 26 Two stage prototype second iteration schematic.

Differences between the first and second iteration of the simple and two stage designs include the addition of a buffer amplifier LM318N to correct the biasing error of the first iteration, individual feedback capacitors for each gain resistor, better power supply regulation and decoupling, and in the two stage case, new op amps.

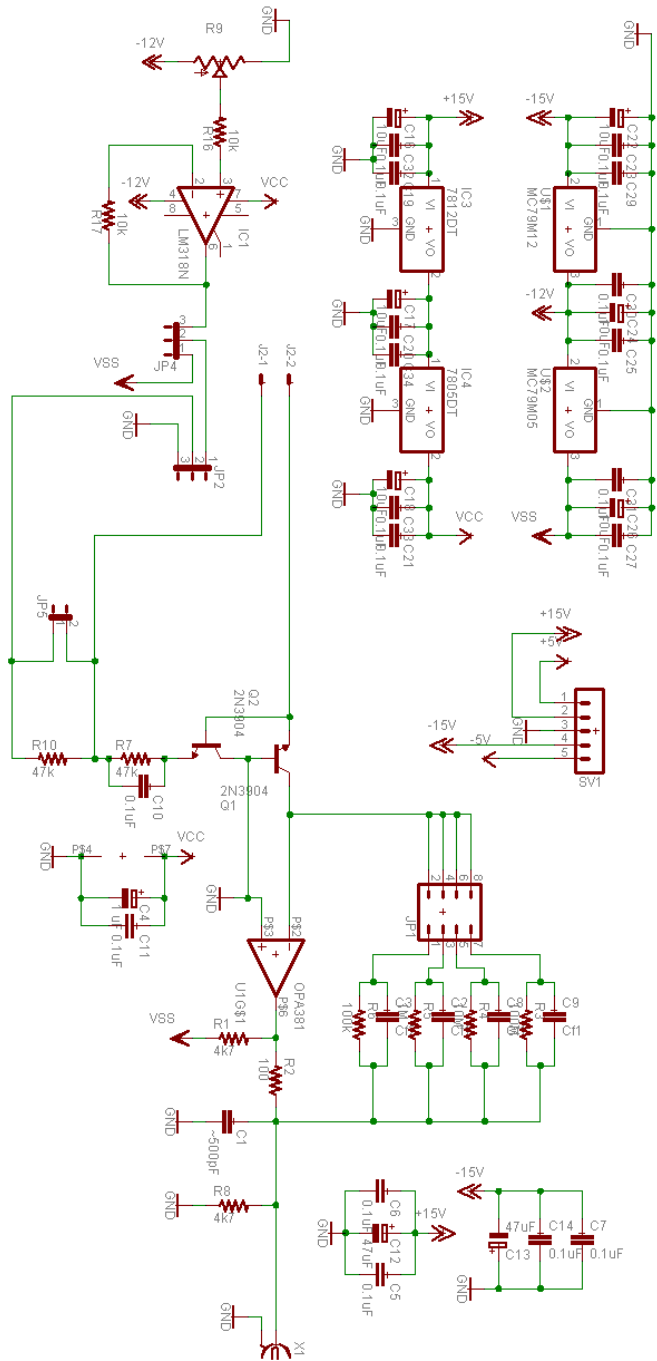


Figure 27 Bootstrapped cascode prototype schematic.

Appendix B: Final Schematic and PCB Layout

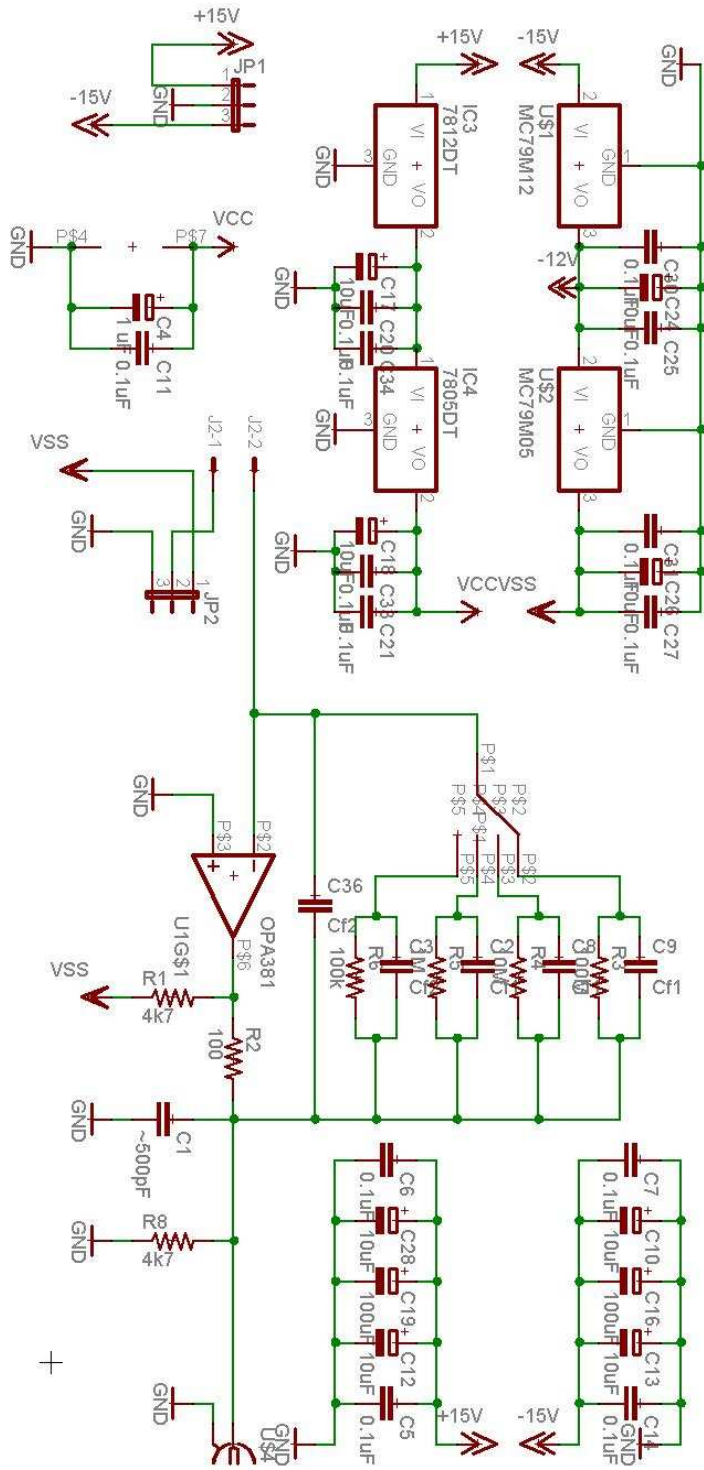


Figure 28 Final circuit schematic.

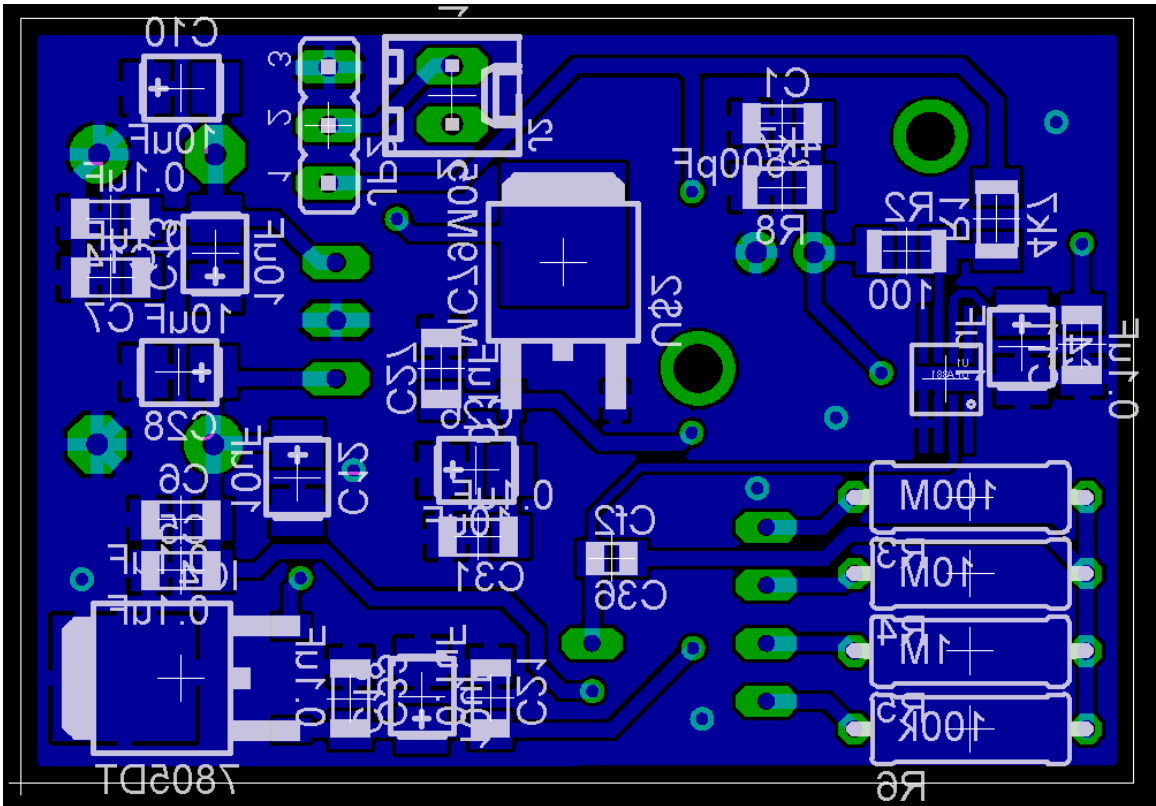
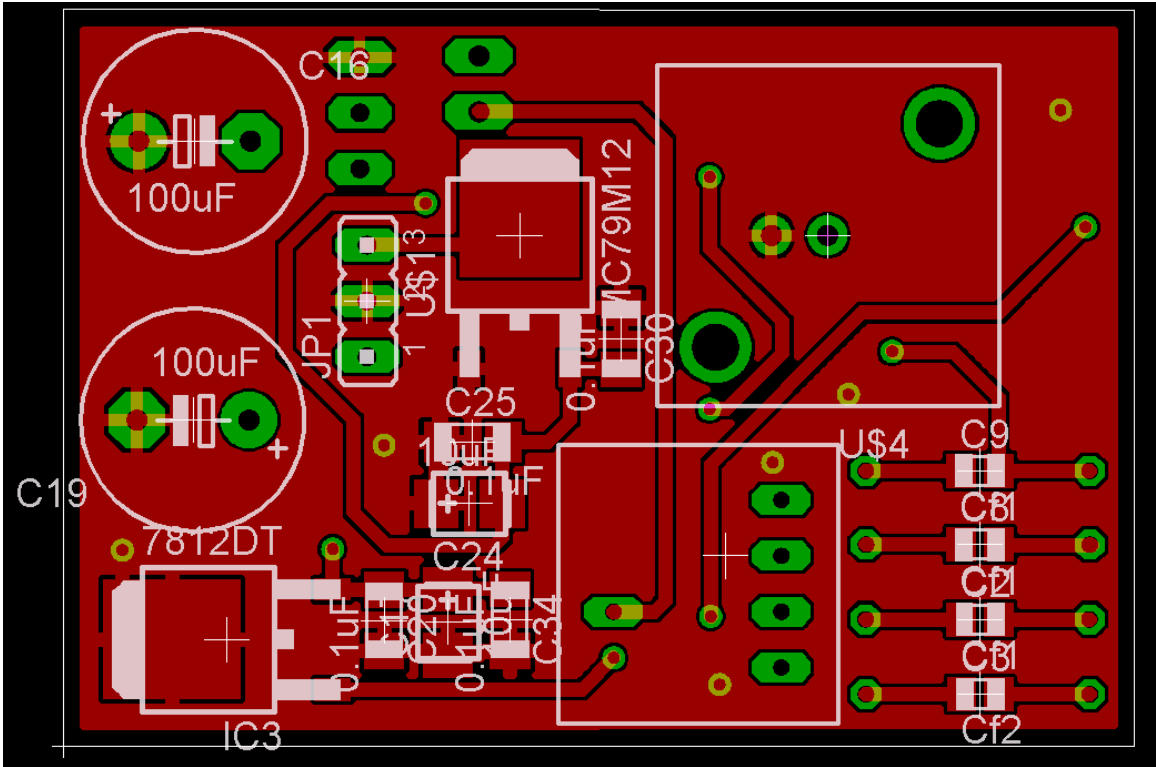


Figure 29 Final PCB layout. Top side in red, bottom (mirrored) in blue.

Appendix C: Laser Driver Board

The laser driver was built to accept an input current on one input and transmit it directly to the laser, and accept an AC voltage on a second input and modulate the laser directly. It was designed to work specifically with the custom built current source available for driver the laser. To avoid having the current source absorb all the AC voltage applied to the AC input, an inductor was placed in series with the current input. The schematic is shown below in Figure 30.

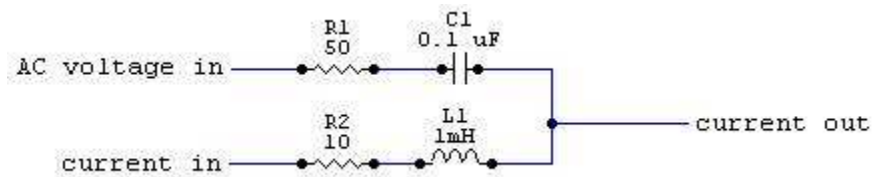
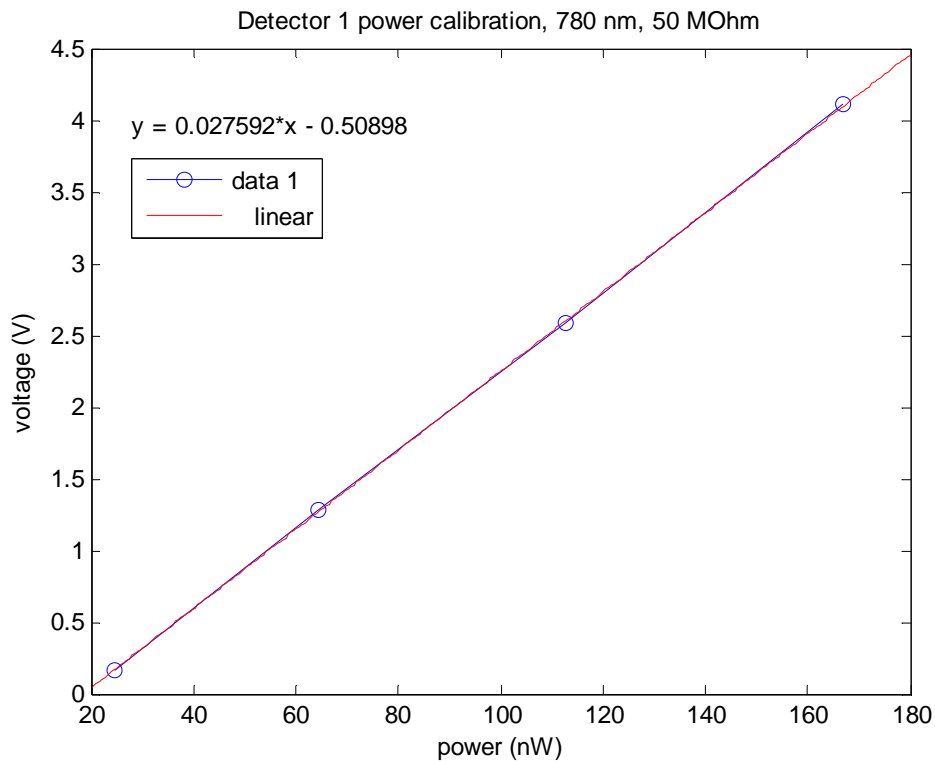
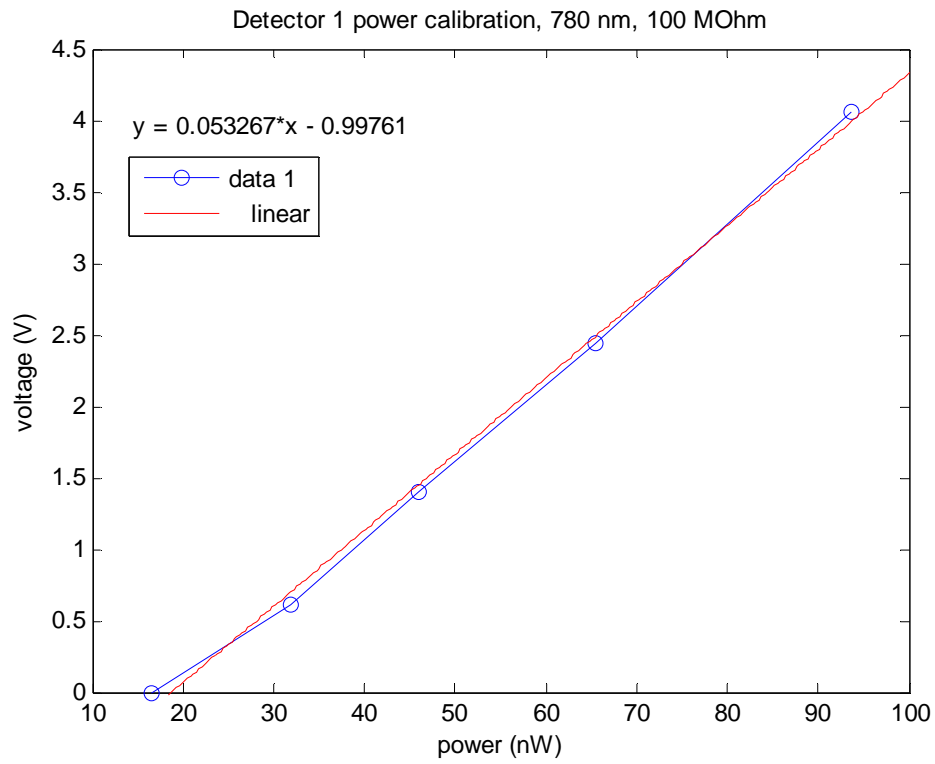


Figure 30 Laser driver schematic.

The board used was modified from a previous similar laser driver. The AC voltage input was not useful at low frequencies, where, despite the inductor, the voltage would be absorbed by the current driver connected to the “current in” input. To avoid this problem, at low frequency (less than approximately 50 kHz) the AC voltage source was connected to the bandwidth limited AC modulation input on the current driver, and at higher frequencies it was connected to the AC voltage in input on the laser driver. In both cases, the amplitude of modulation on the laser current was frequency dependent. To eliminate this unknown variation, the frequency response measurements used a New Focus 125 MHz photodetector as a reference, as described in Section 2.4.3.

Appendix D: Power Calibration Curves



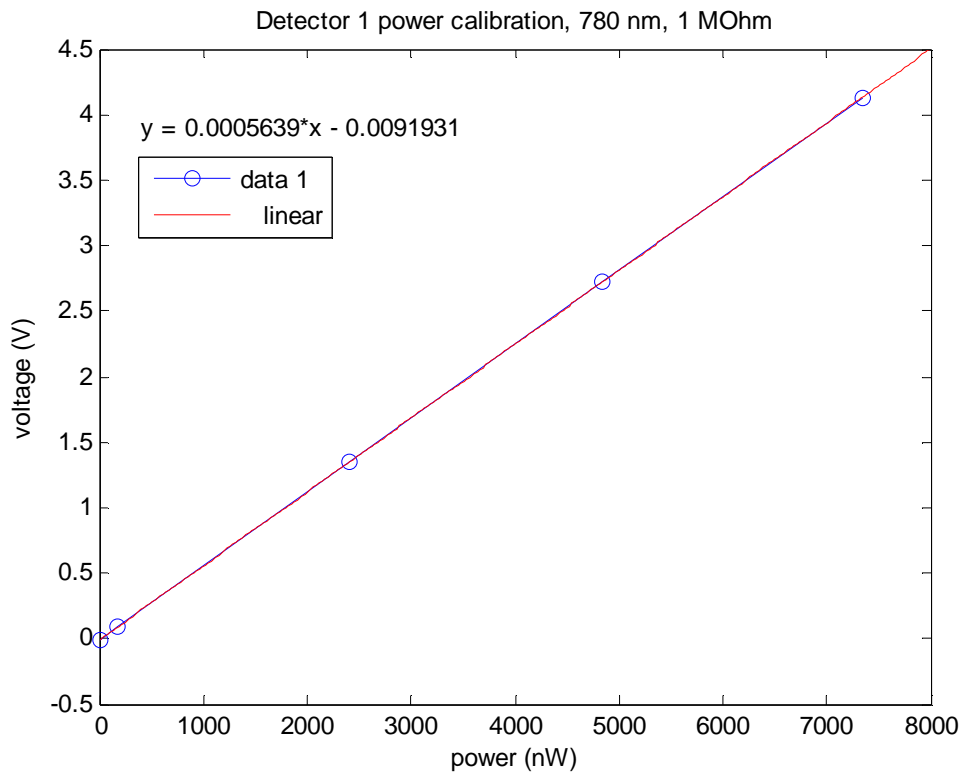
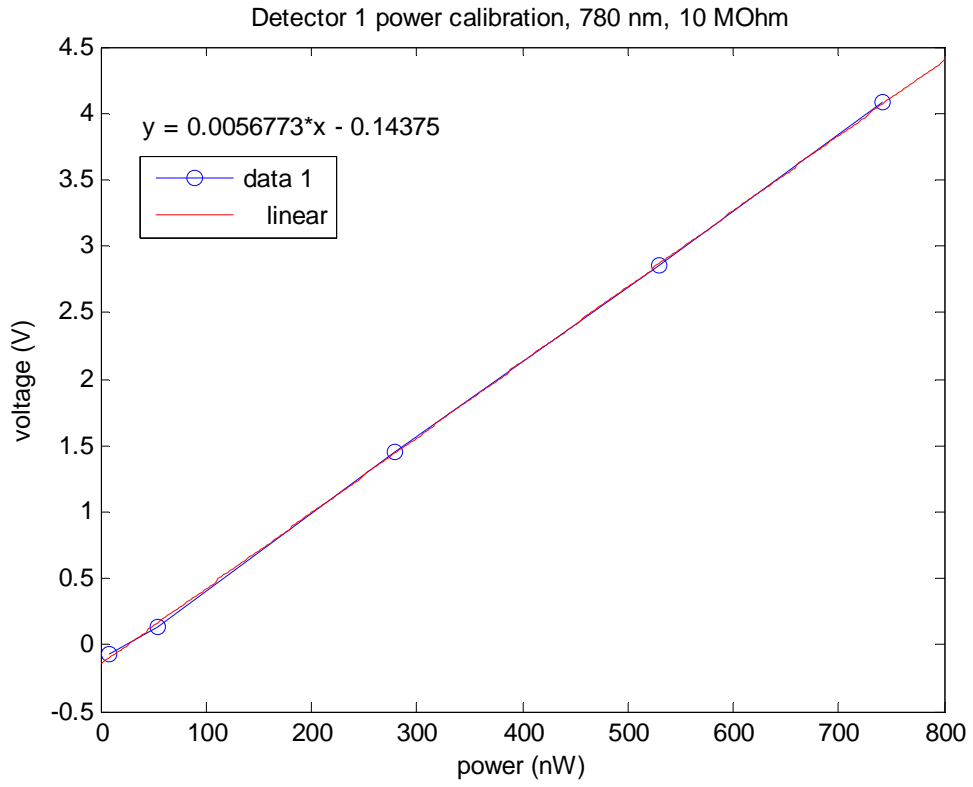
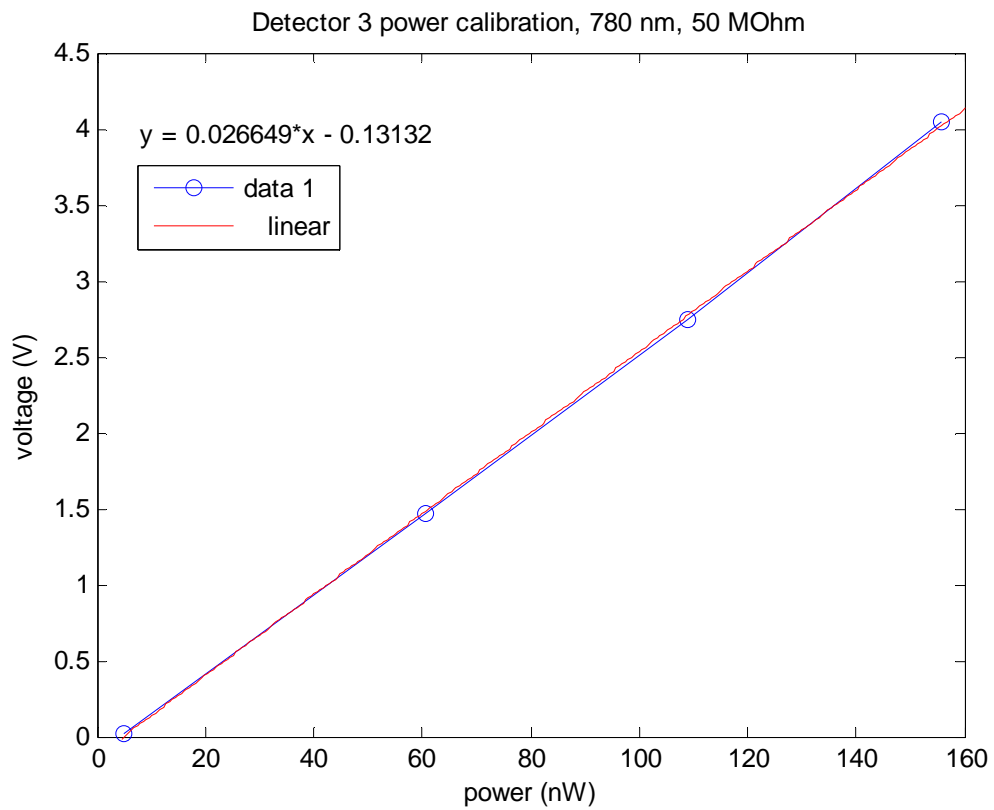
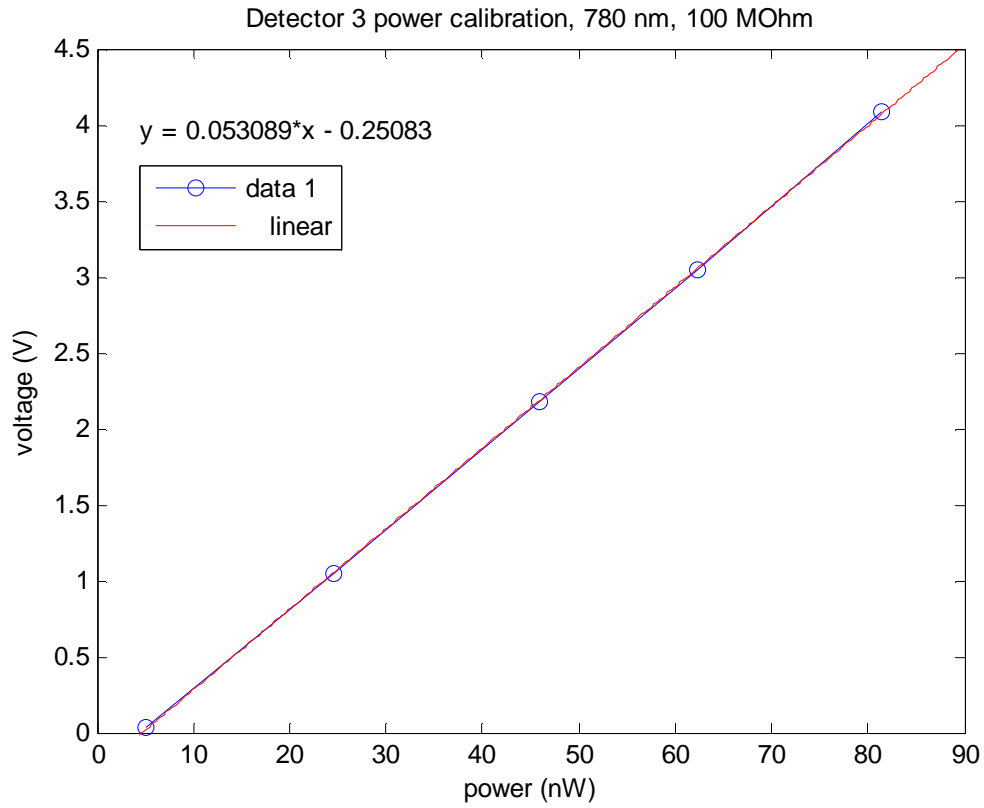


Figure 31 Detector 1 Power Calibration Curves



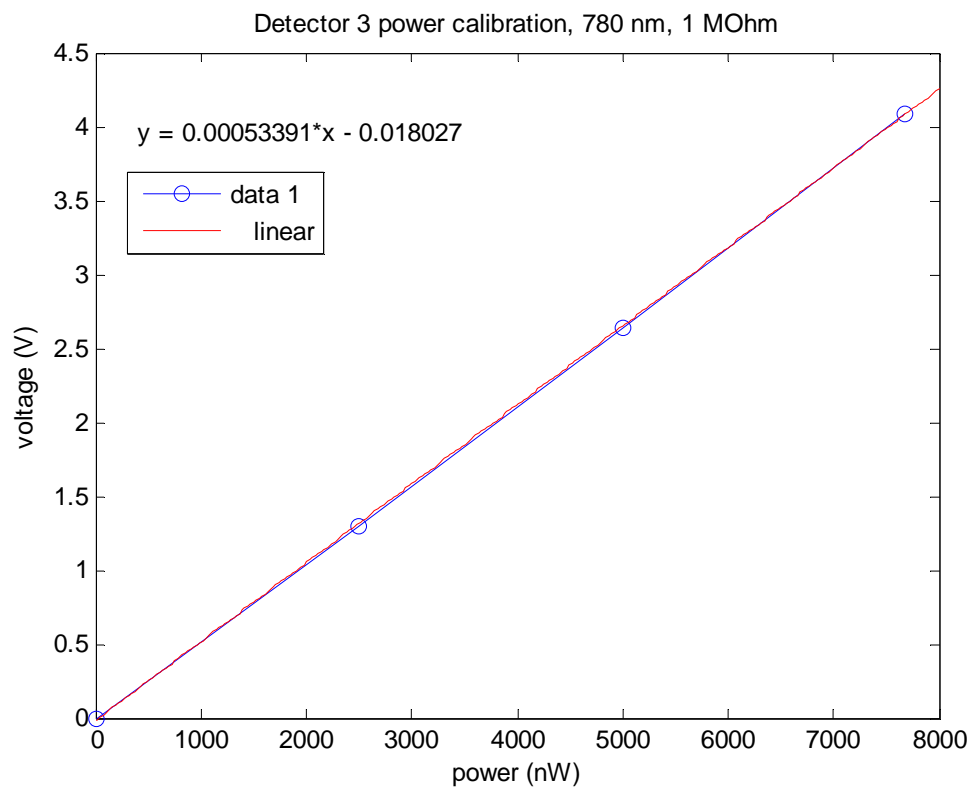
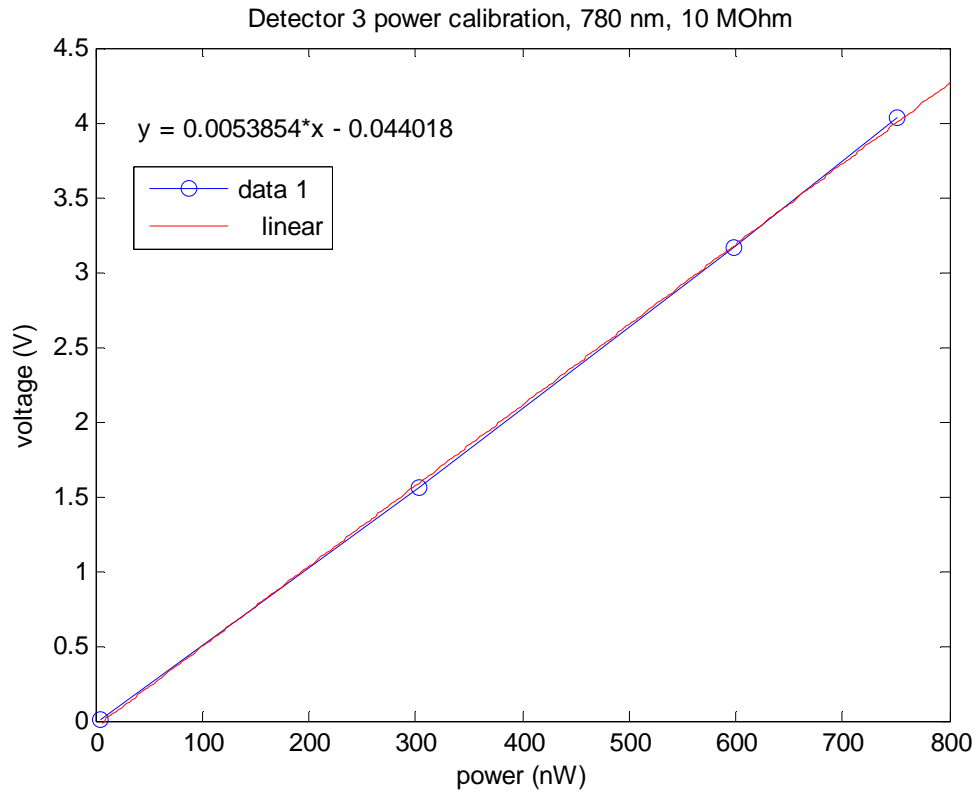
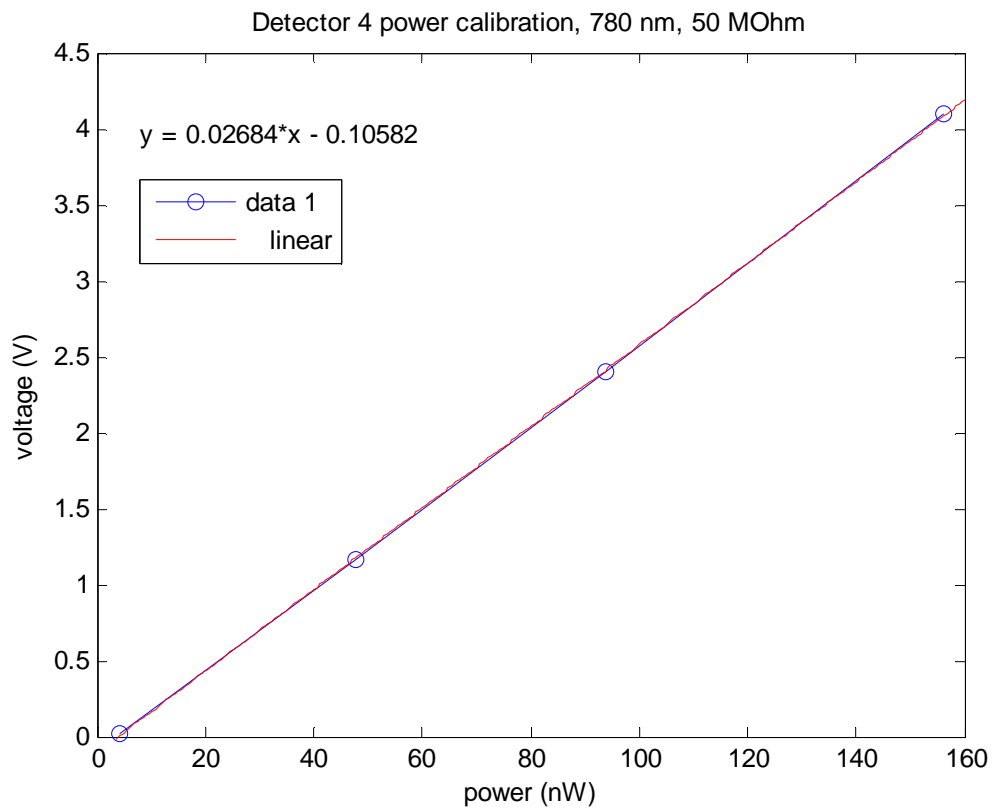
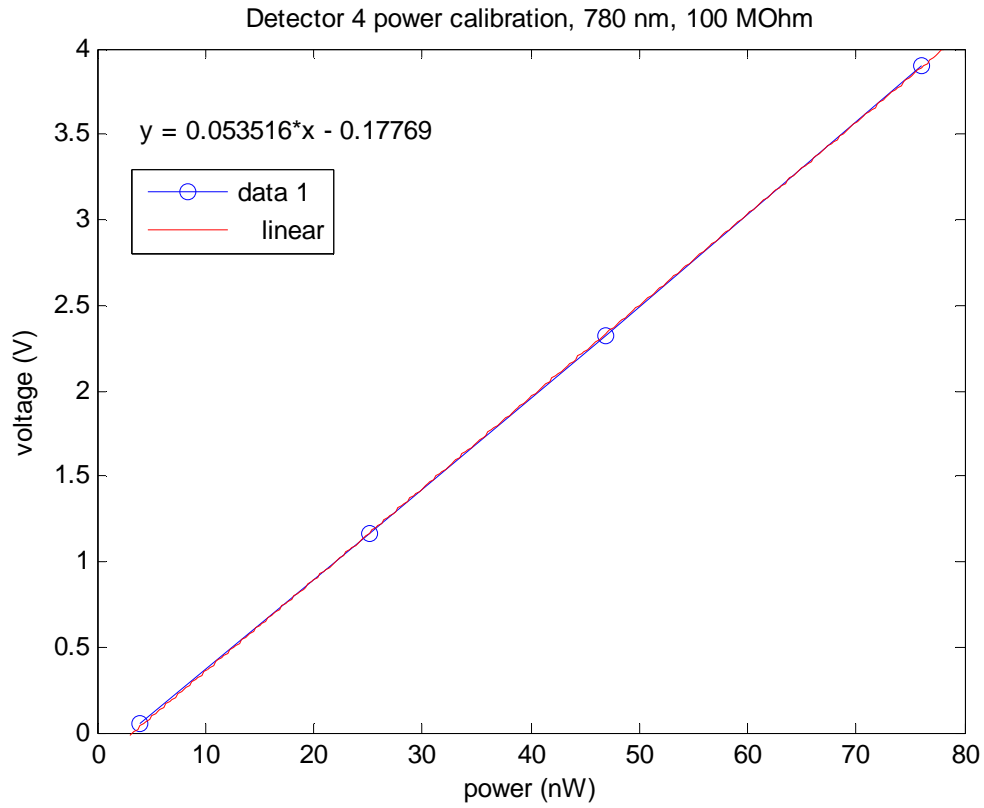


Figure 32 Detector 3 Power Calibration Curves



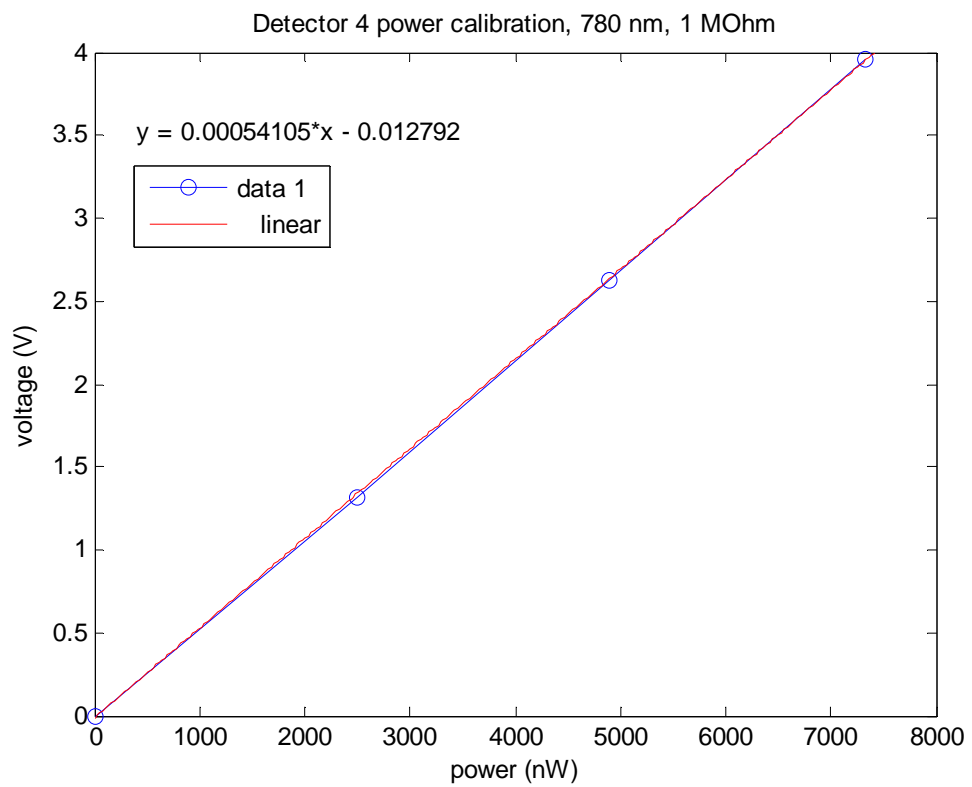
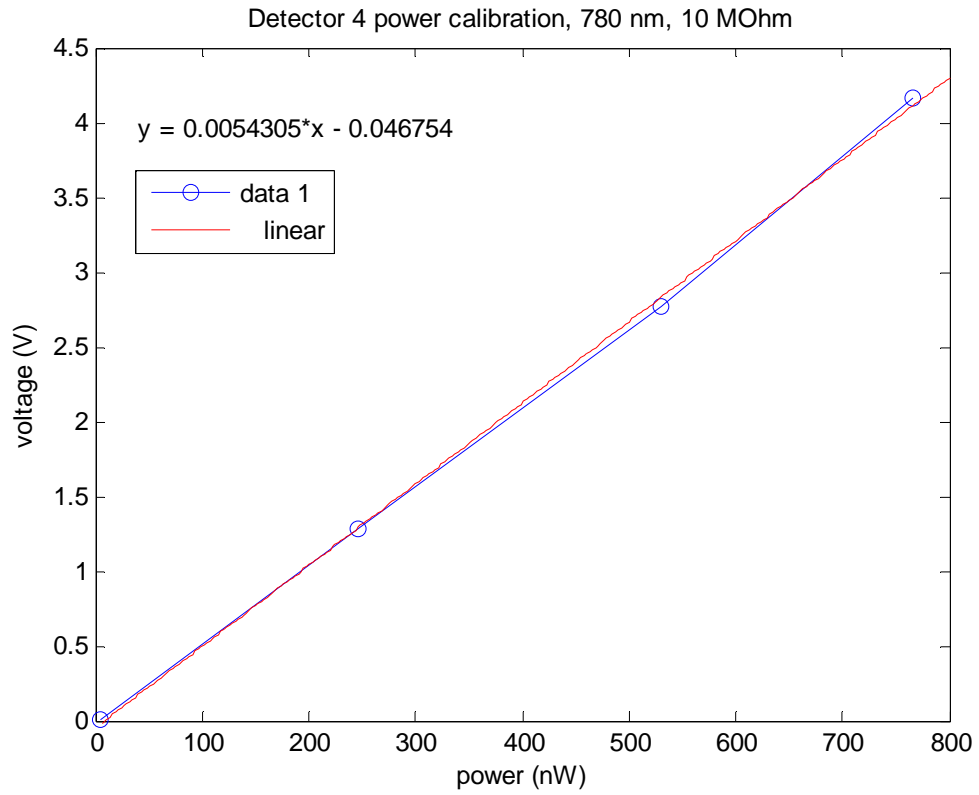
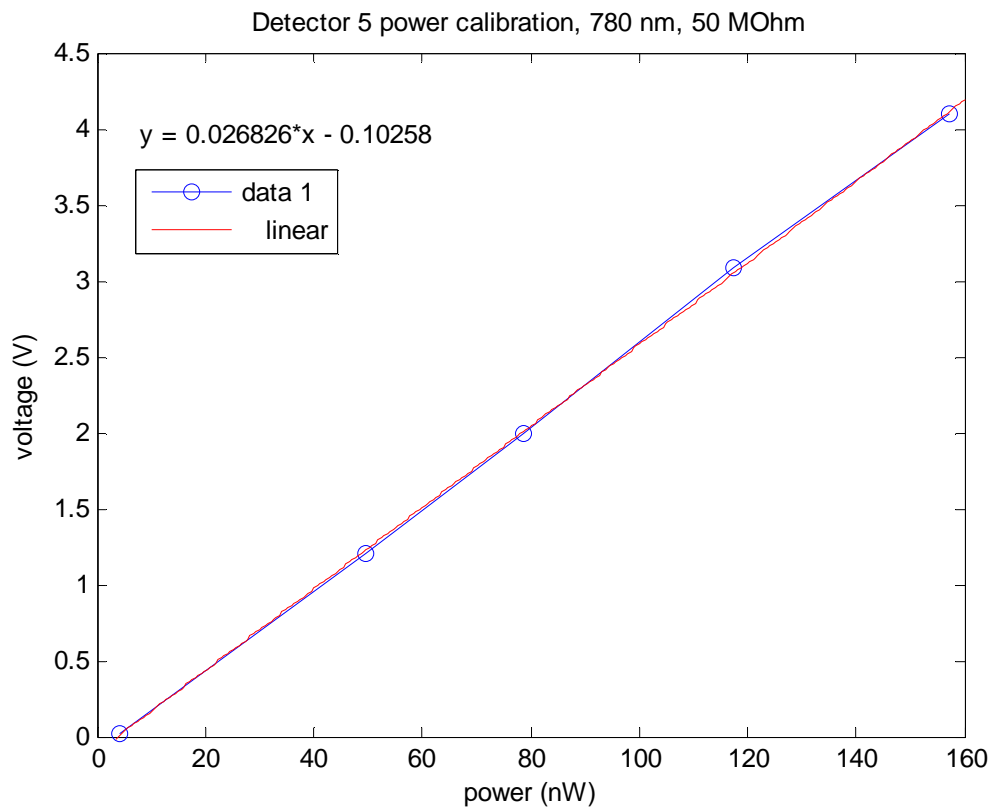
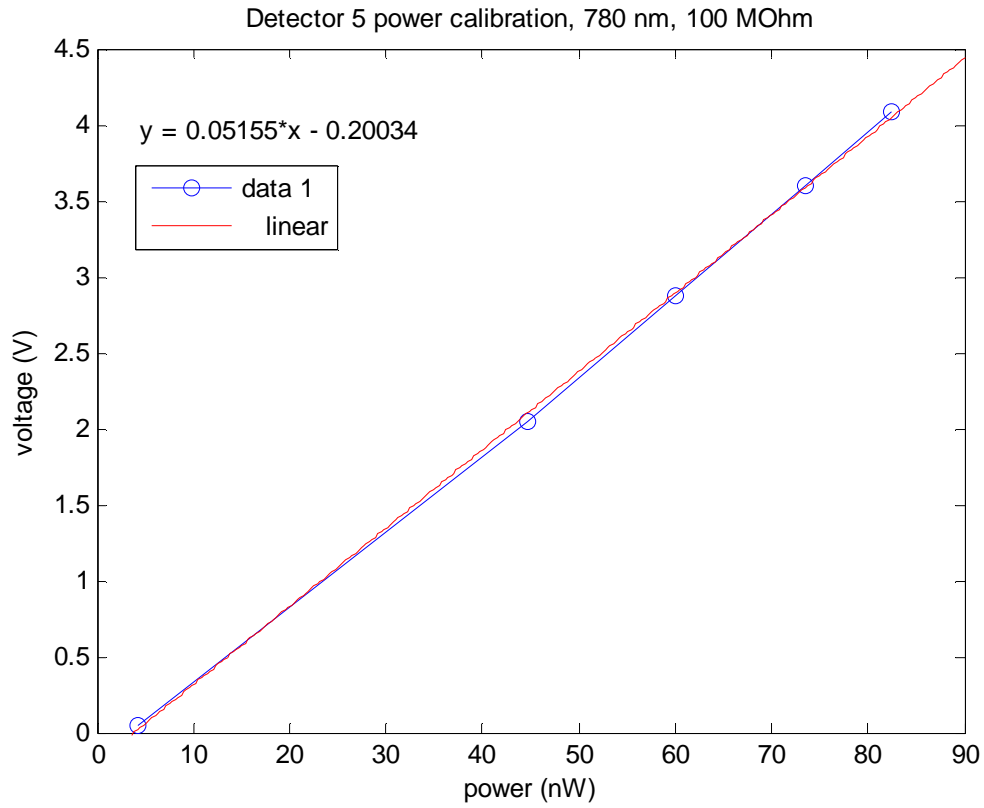


Figure 33 Detector 4 Power Calibration Curves



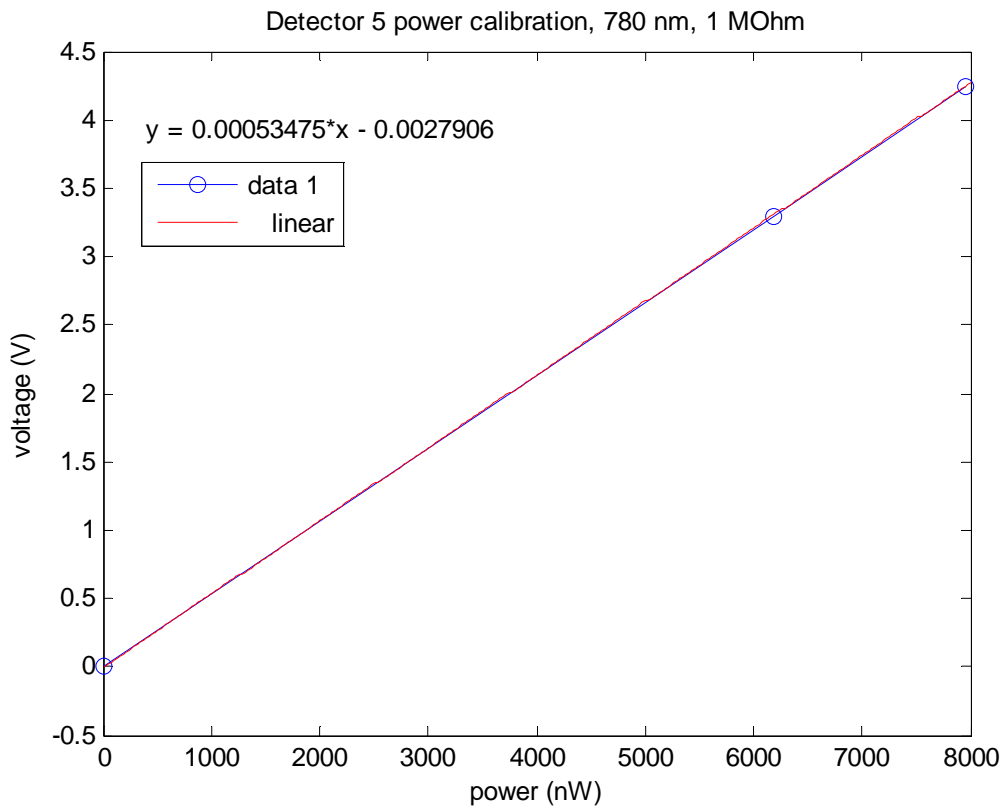
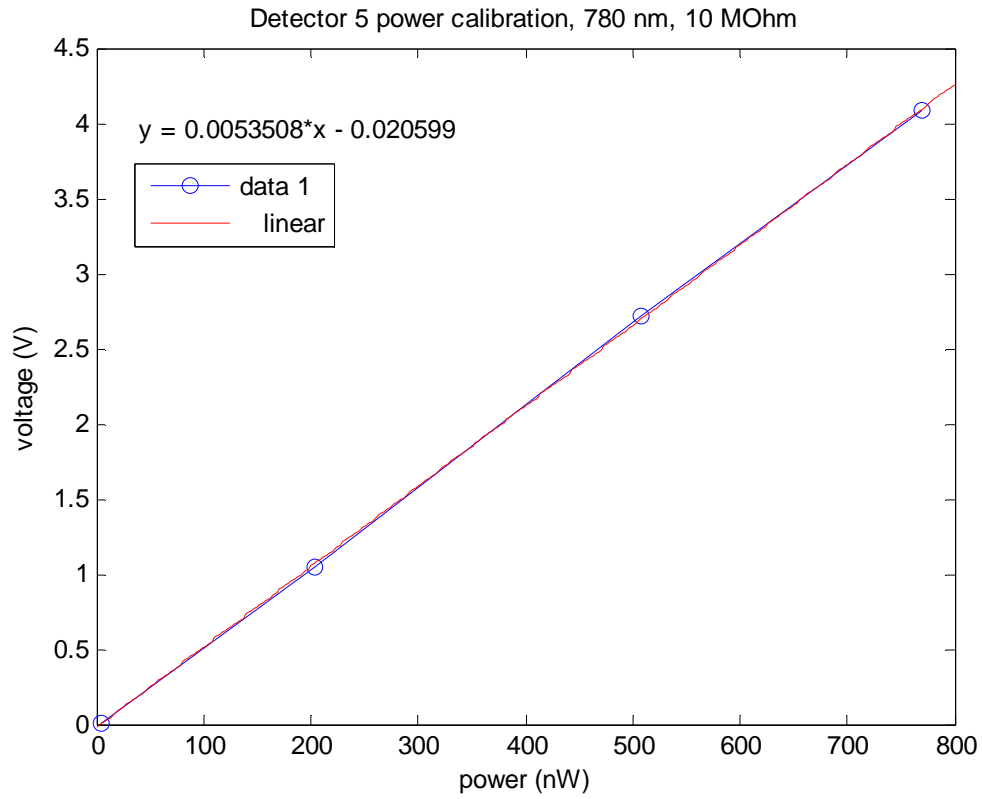
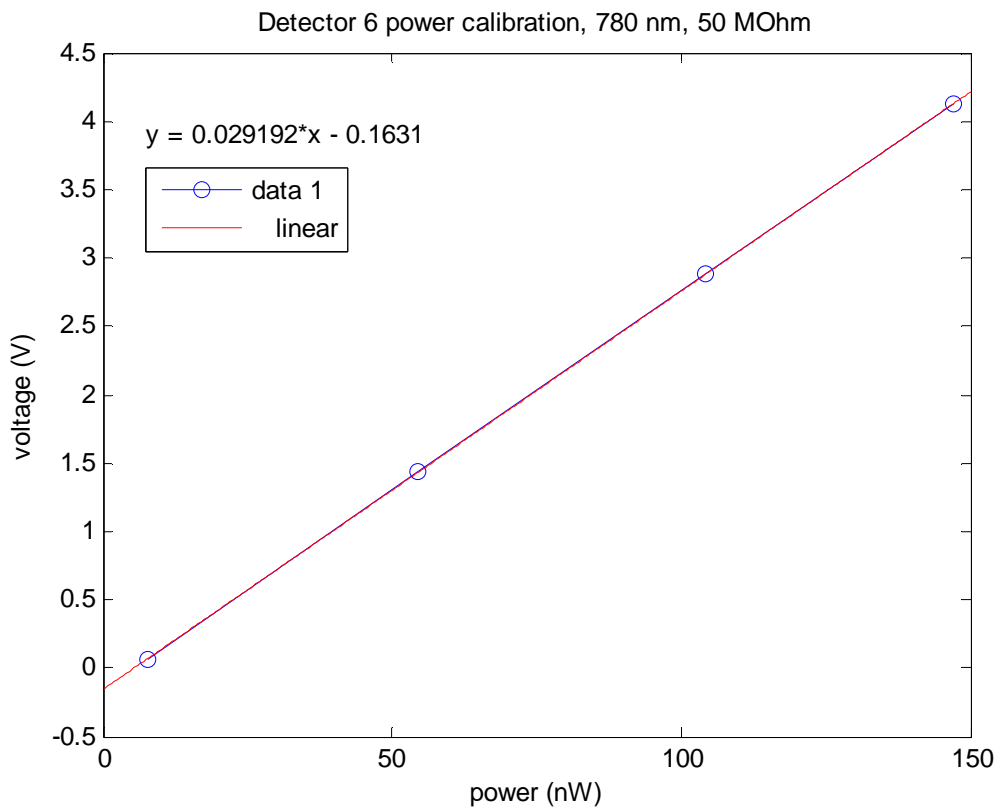
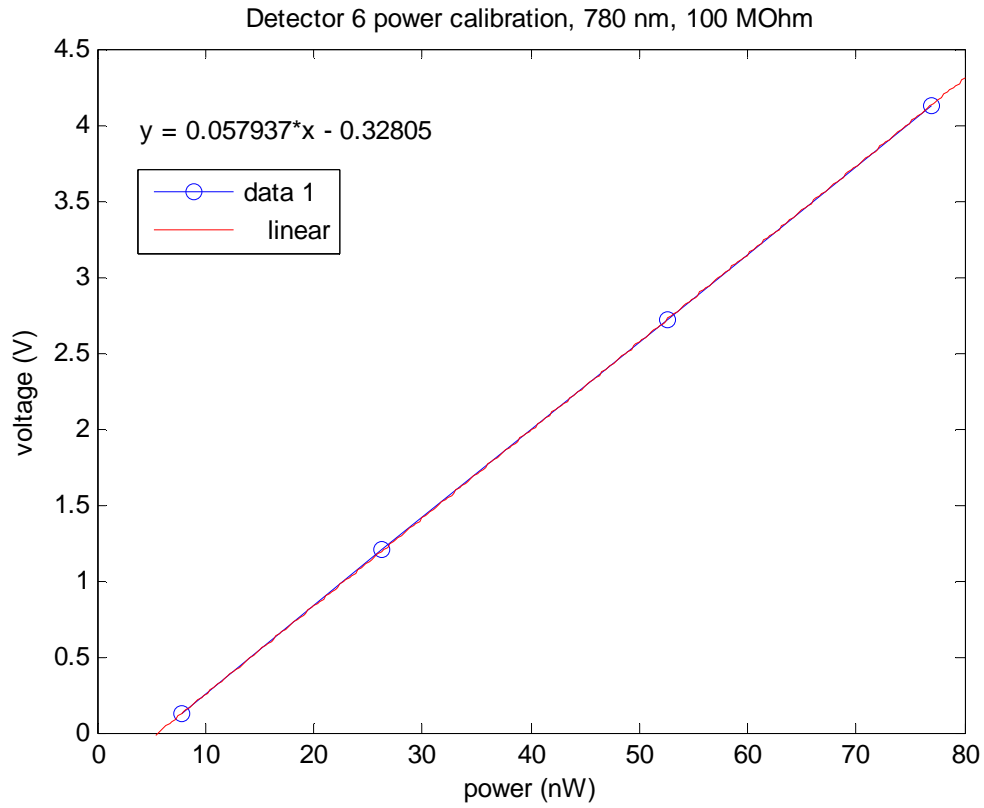


Figure 34 Detector 5 Power Calibration Curves



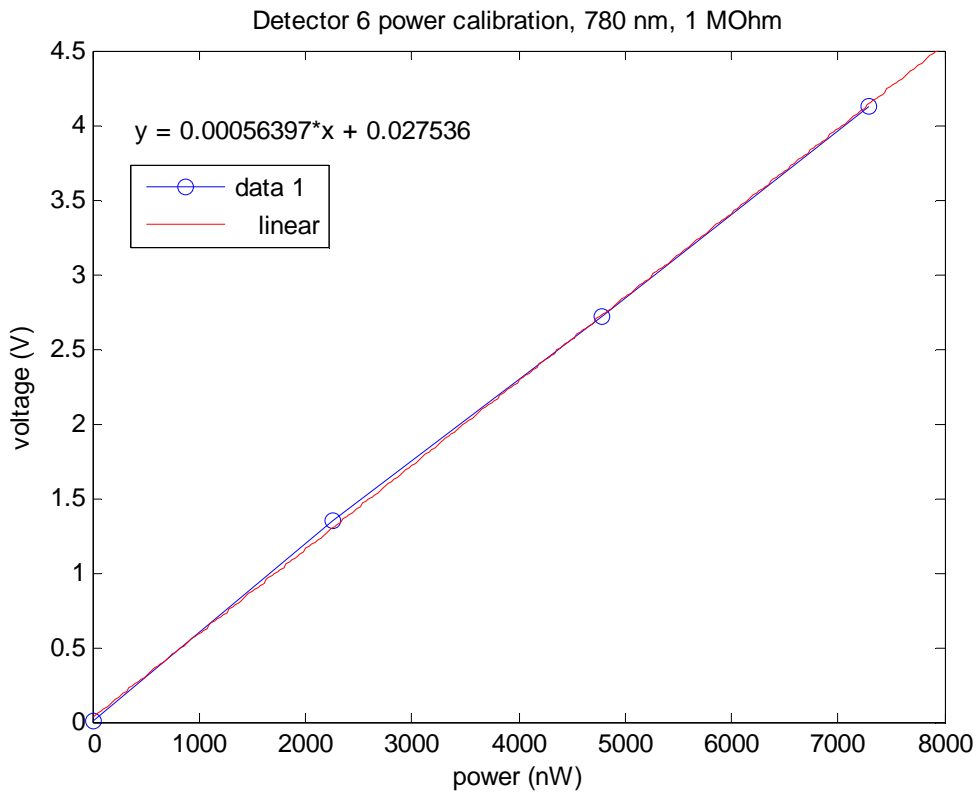
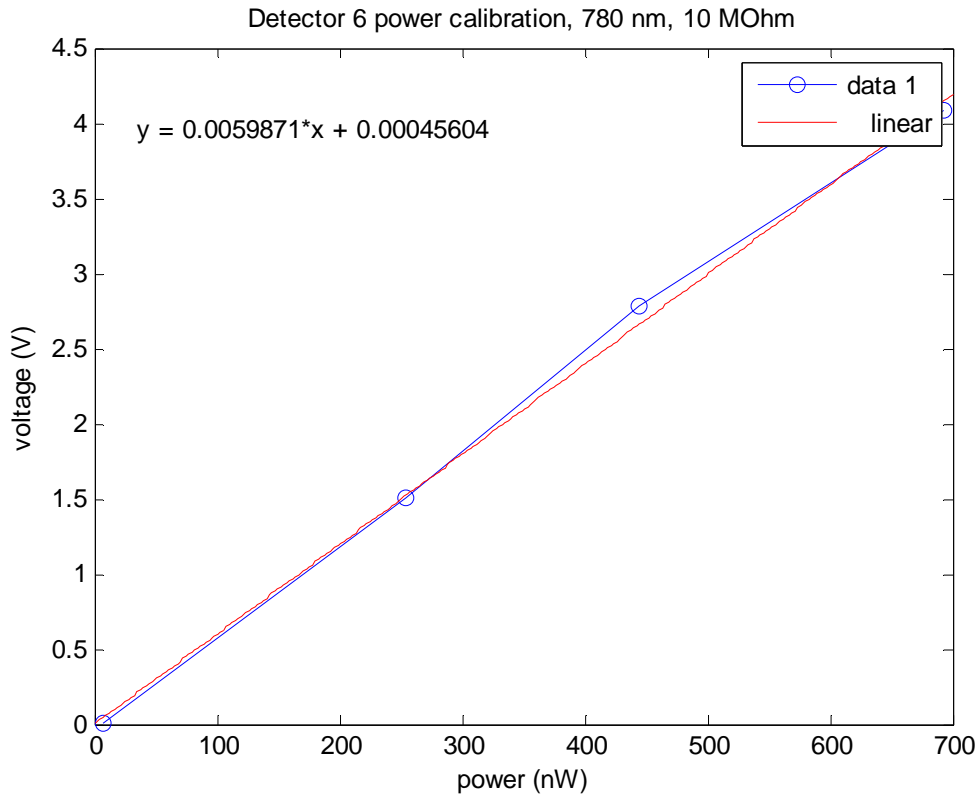
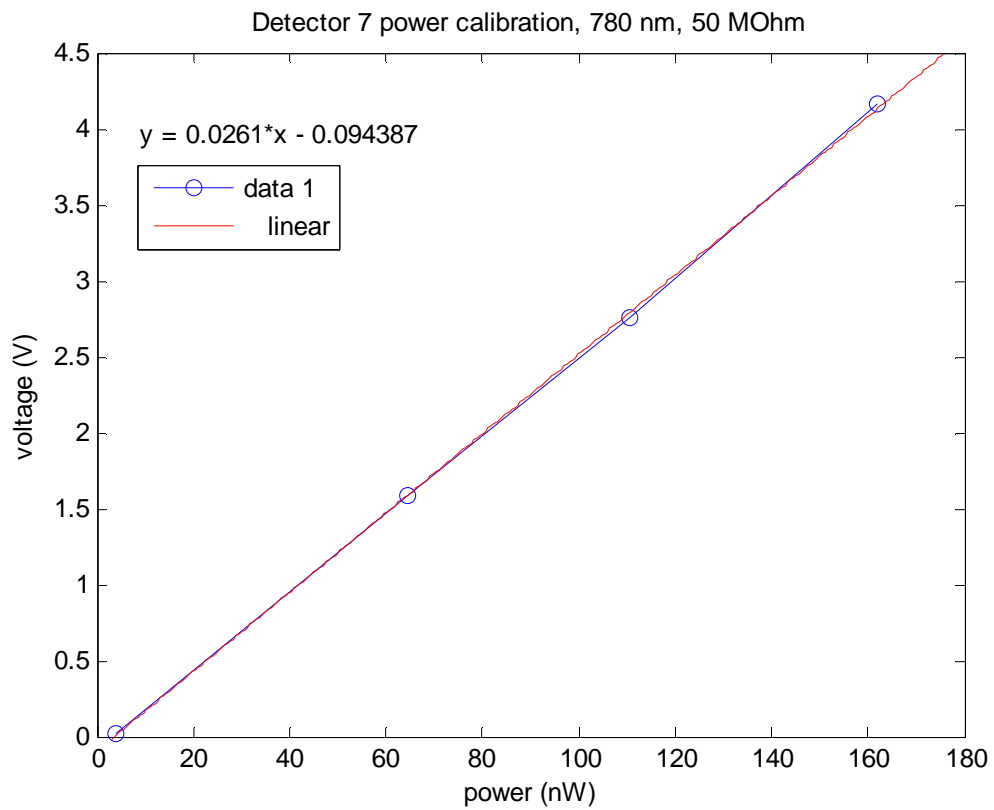
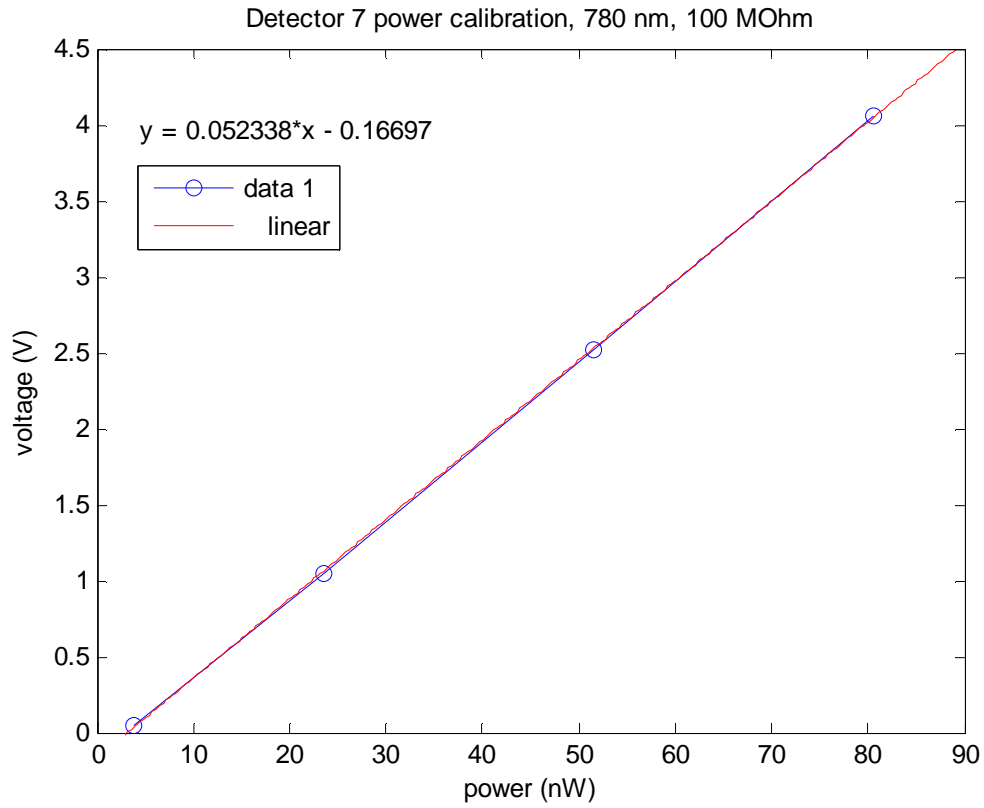


Figure 35 Detector 6 Power Calibration Curves



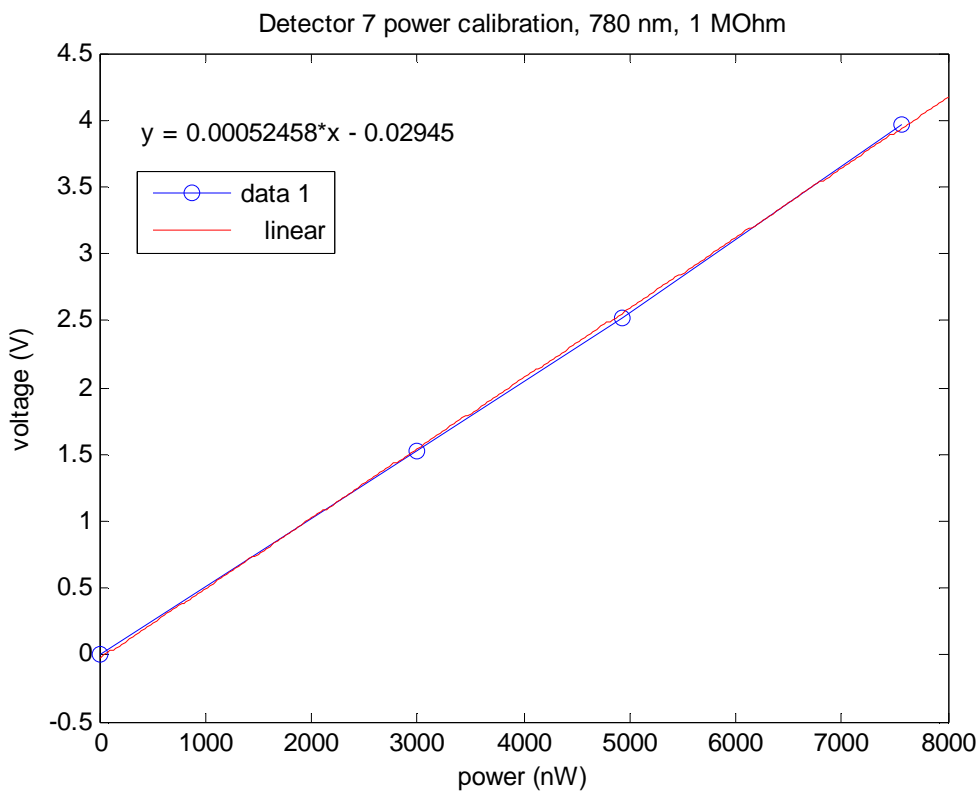
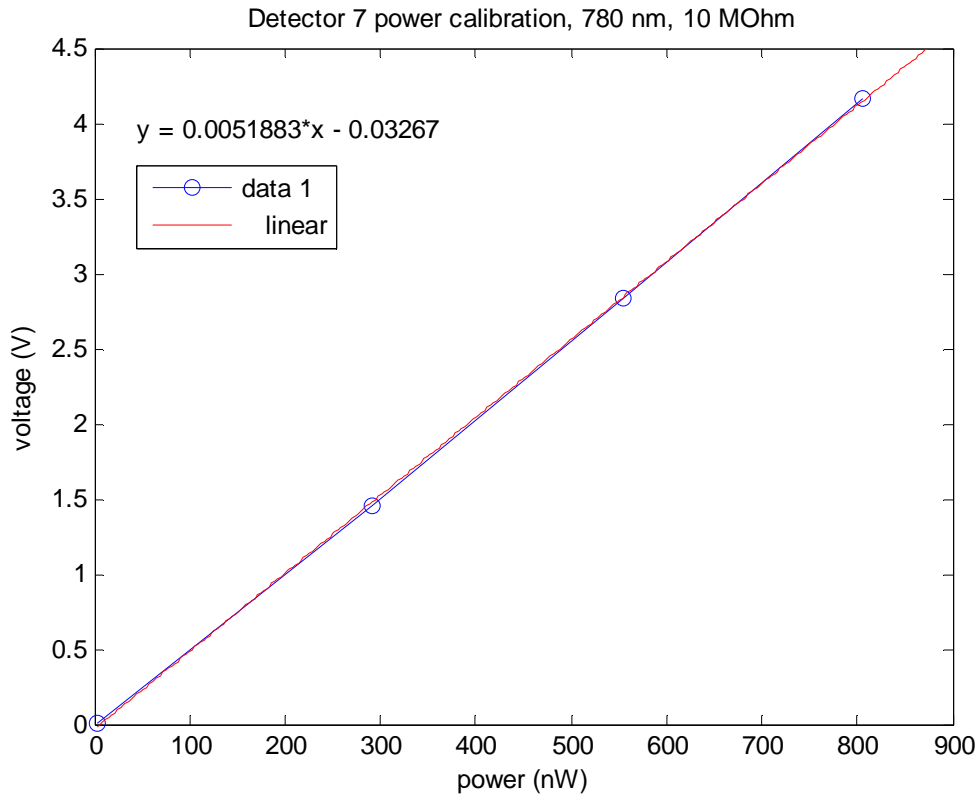
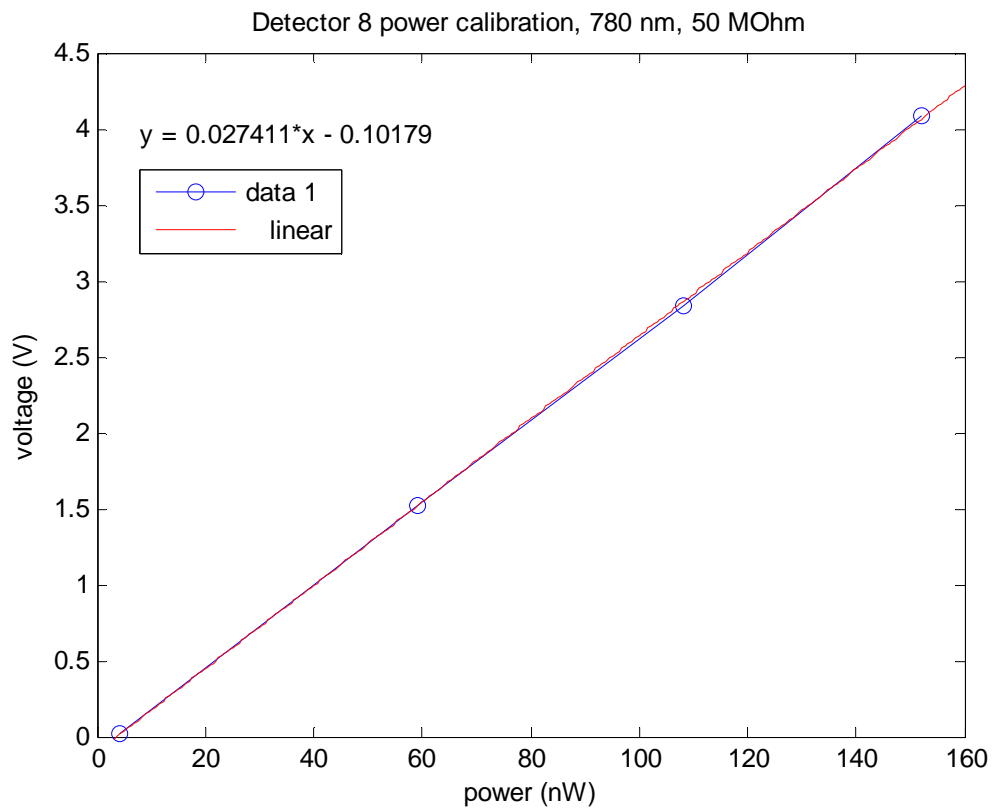
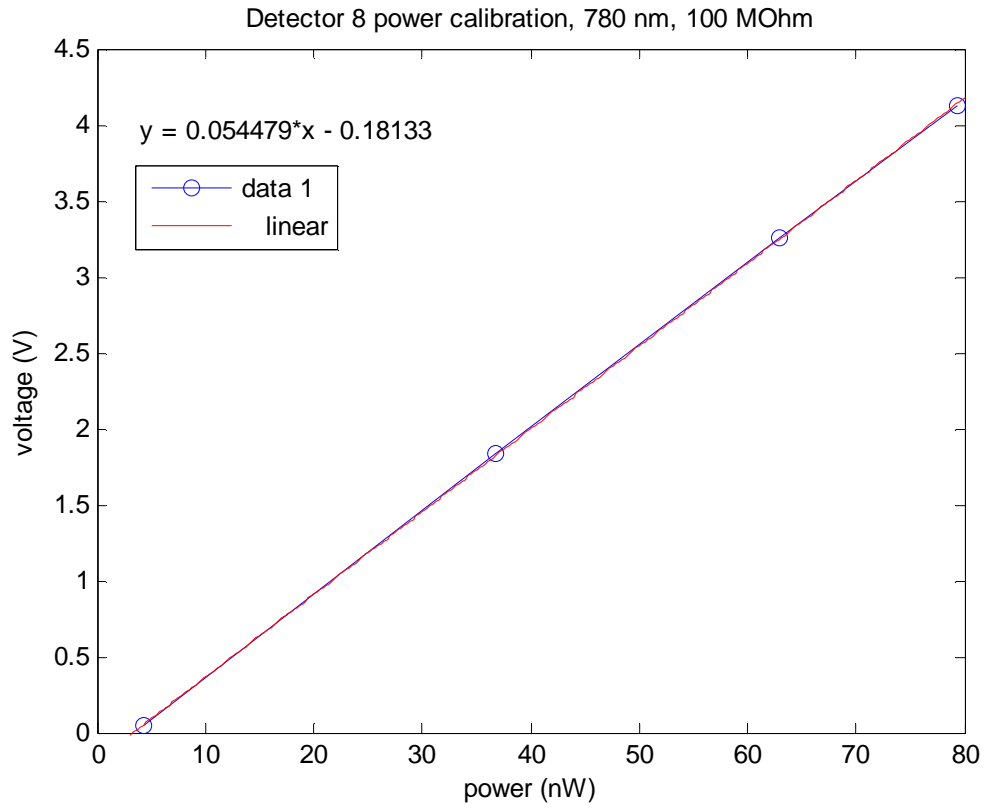


Figure 36 Detector 7 Power Calibration Curves



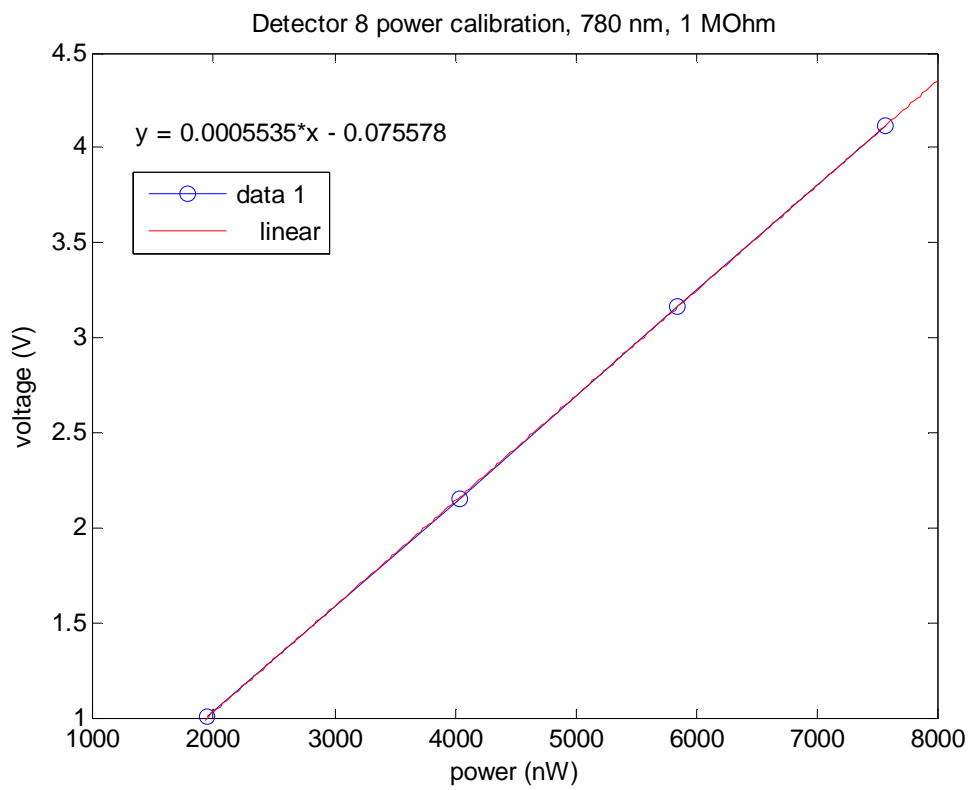
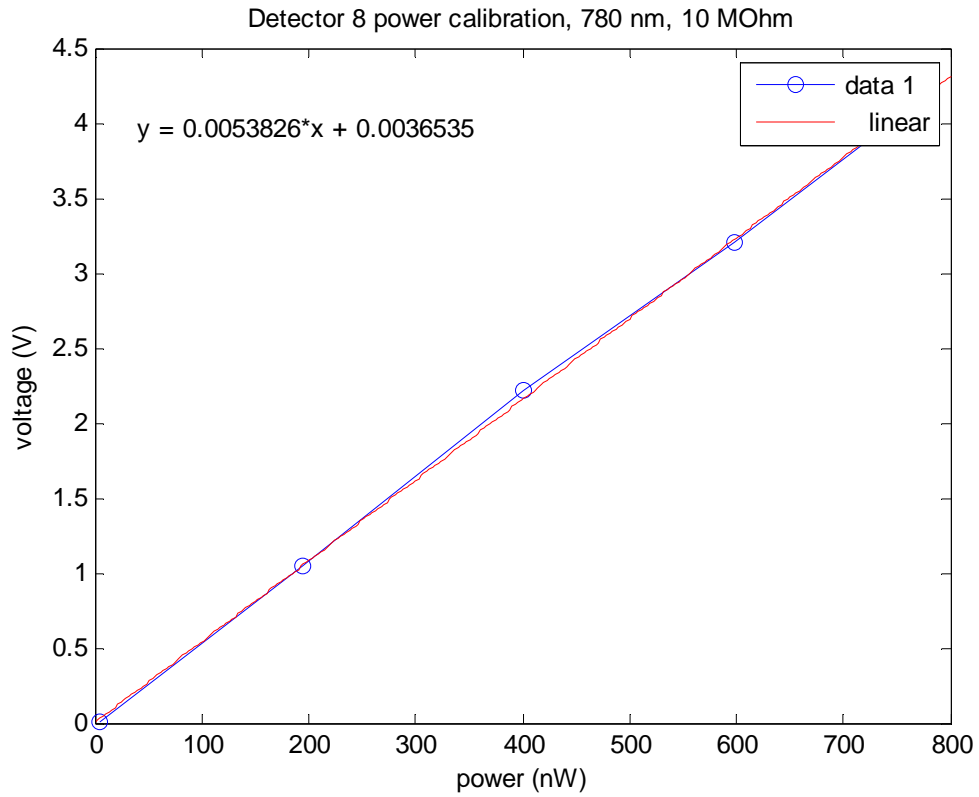


Figure 37 Detector 8 Power Calibration Curves

References

1. Graeme, Jerald. "FET op amps convert photodiode outputs to useful signals". EDN, October 29th 1987, 205-220
2. Tony Wang, Barry Erhman. "Compensate Transimpedance Amplifiers Intuitively". Texas Instruments Application Report, SBOA055A, March 1993, Revised March 2005.
3. Thorlabs FDS1010 Si Photodiode datasheet. 2739-S01 Revision B. April 30th 2001.
4. Texas Instruments OPA381 OPA2381 datasheet. SBOS313B. August 2004, Revised November 2004.
5. Texas Instruments OPA656 datasheet. SBOS197B. December 2001, Revised May 2004.
6. Report titled "Photodiode Project" written by Dr. James Booth detailing his past work on the project.
7. Meetings with Dr. Kirk Madison, Dr. James Booth, and Dr. Bruce Klappauf on September 8th and September 12th 2008
8. Pease, Bob. "What's All This Transimpedance Amplifier Stuff, Anyhow? (Part 1)". electronic design online, January 8th 2001.
<<http://electronicdesign.com/Articles/Index.cfm?AD=1&ArticleID=4346>>
9. Wikipedia Magneto-Optical Trap article, September 18th 2008.
< http://en.wikipedia.org/wiki/Magneto-optical_trap>
10. Hobbs, Philip C.D. "Photodiode Front Ends: The Real Story". Optics and Photonics News, April 2001, 44-47.
11. Ying-Cheng Chen, Yean-An Liao, Long Hsu, Ite A. Yu. "Simple technique for measuring the number of atoms in a magneto-optical trap". APS Physics, Revision A, Volume 64, Issue 3, August 13 2001.
12. Hobbs, Philip C.D. "Building Electro-Optical Systems: Making it all Work". John Wiley & Sons, Inc, 2000.
13. New Focus Visible 125 MHz photoreceiver product page, January 11th 2009.
<<http://www.newfocus.com/products/?navId=3&theView=modelGroupDetail&productLineId=3&productGroupId=137&modelGroupId=1054>>.

14. Paul Horowitz, Winfield Hill. "The Art of Electronics". Cambridge University Press, 1980.
15. Analog Devices AD8655 datasheet. D05304-0-6/05(A), Revision A. 2005.
16. Analog Devices AD8027 datasheet. C03327-0-3/05(C), Revision C. 2005.
17. Analog Devices AD8625/AD8626/AD8627 datasheet. C03023-0-11/04(C), Revision C. 2004.
18. Analog Devices AD8221 datasheet. D03149-0-9/07(B), Revision B. 2007.
19. Texas Instruments OPA380 OPA2380 datasheet. SBOS291G. November 2003, Revised September 2007.